





Squeezing and quantum control of the antiferromagnetic magnon pseudospin

Anna-Luisa E. Römling ^{1,2}, Johannes Feist ^{1,2}, Francisco J. García-Vidal ^{1,2} and Akashdeep Kamra ^{3,1,2}

¹*Departamento de Física Teórica de la Materia Condensada, Universidad Autónoma de Madrid, E-28049 Madrid, Spain*

²*Condensed Matter Physics Center (IFIMAC), Universidad Autónoma de Madrid, E-28049 Madrid, Spain*

³*Department of Physics and Research Center OPTIMAS, Rheinland-Pfälzische Technische Universität Kaiserslautern-Landau, 67663 Kaiserslautern, Germany*



(Received 6 June 2025; revised 24 November 2025; accepted 26 November 2025; published 19 December 2025)

Antiferromagnets have been shown to harbor strong magnon squeezing in equilibrium, making them a potential resource for quantum correlations and entanglement. Recent experiments have also found them to host coherently coupled magnonic excitations forming a magnon pseudospin, in analogy to electronic spin. Here, we delineate the quantum properties of the antiferromagnetic magnon pseudospin by accounting for spin nonconserving interactions and going beyond the rotating wave approximation. Employing concrete examples of nickel oxide and hematite, we find strong squeezing of the magnon pseudospin highlighting its important role in determining the eigenmode quantum properties. Via ground-state quantum fluctuations engineering, this pseudospin squeezing enables an enhancement and control of coupling between the magnonic modes and other excitations. Finally, we evaluate the quantum superpositions that comprise a squeezed pseudospin ground state and delineate a qubit spectroscopy protocol to detect them. Our results are applicable to any system of coupled bosons and thus introduce quantum fluctuations engineering of a general bosonic pseudospin.

DOI: [10.1103/qjm2-d19g](https://doi.org/10.1103/qjm2-d19g)

I. INTRODUCTION

As per the Heisenberg uncertainty [1] relation, complementary physical observables cannot be measured precisely at the same time. Squeezed states harbor reduced quantum fluctuations or uncertainty in a physical observable at the expense of an increased noise in its complementary counterpart [2–4]. For light, such states have thus been exploited for measurements with a sensitivity beyond what is allowed by the quantum ground state and coherent states as produced by lasers [4–7]. Contained implicitly in this engineering of quantum fluctuations is entanglement, which has been utilized for teleportation [8–10]. The generality of the concept has enabled the realization of squeezed states with one boson mode [11–13], two boson modes [14,15], and atomic ensembles of spin [16–26], with each platform harboring unique phenomena and advantages. However, the squeezed states in these examples are nonequilibrium in nature and decay rapidly as the generating mechanism is switched off.

Ordered magnets and their excitations—magnons—have recently been shown to harbor squeezed states and excitations in equilibrium, thereby uncovering fresh advantages and phenomena [27–35]. Magnons have already proven promising for an information transport and processing paradigm harnessing the unique potential of spin and bosonic excitations, with several phenomena and devices demonstrated [29,36–42]. Antiferromagnetic magnons are particularly exciting due to their typically high frequencies and equilibrium squeezing larger than what has been feasible with light [29,30]. Furthermore, they come in pairs of spin-up and spin-down modes, much like the spin of an electron. Coherently coupled spin-up and spin-down modes enable a new degree of freedom—magnon pseudospin—capable of capitalizing on

the positive features of fermionic electrons, bosonic magnons, and squeezing [43,44]. The recent observation of the magnon Hanle effect [44] has demonstrated experimental control over the magnon pseudospin and uncovered a wide range of fresh opportunities [45–50].

Inspired by its usefulness in several newly discovered spin transport phenomena, here, we uncover some quantum properties of the antiferromagnetic magnon pseudospin focusing on its squeezing and the concomitant eigenmode quantum superpositions. We demonstrate that its mathematical similarity to spin offers an equilibrium realization of spin squeezing via unequal quantum fluctuations in orthogonal pseudospin components. This pseudospin squeezing can be conveniently controlled via typical spintronic controls, such as an applied magnetic field. At the same time, the underlying bosonic nature of the pseudospin enables fresh coupling enhancement and control opportunities akin to similar effects observed recently in, for example, trapped ion systems [51]. The quantum superpositions of a squeezed state that underlie these phenomena are then evaluated for the magnon pseudospin and a protocol for detecting them via a qubit is theoretically demonstrated. Employing experimentally measured parameters, we quantify the pseudospin squeezing in nickel oxide and hematite, and note the recently discovered van der Waals magnets to naturally embody our studied coupled magnon pseudospin-qubit system [52,53].

II. ANTIFERROMAGNETIC MAGNON PSEUDOSPIN

We consider a bipartite antiferromagnetic insulator (AFM) [54,55] with exchange as the dominant interaction. In the Néel ordered classical ground state, the two spin sublattices are fully and oppositely polarized. We denote sublattice

A (*B*) as the sublattice polarized along the negative (positive) *z* direction. Excitations on sublattice A (*B*) are delocalized spin-flips with spin +1 (−1). However, strong exchange coupling between the sublattices induces correlations and intrinsic squeezing, quantified by a parameter *r*, in the quantum fluctuations of the sublattice spins [28]. Because of this, excitations of the AFM are spin-up and spin-down magnonic modes perturbing both sublattices as a superposition of spin-flip states. We consider here the spatially uniform modes (wave vector $\mathbf{k} = \mathbf{0}$), and represent spin-up and spin-down magnonic modes by the bosonic annihilation operators $\hat{\alpha}$ and $\hat{\beta}$.

Accounting for the spin nonconserving (SNC) interactions, coherent magnon-magnon coupling between the modes $\hat{\alpha}$ and $\hat{\beta}$ is obtained, as derived in Appendix A 1. Within the rotating wave approximation (RWA), an assumption we later relax, the magnonic excitations are described by the following Hamiltonian ($\hbar = 1$) [43]:

$$\hat{\mathcal{H}}_{\text{Hyb}} = \omega(\hat{\alpha}^\dagger \hat{\alpha} + \hat{\beta}^\dagger \hat{\beta}) - D_r(\hat{\alpha} \hat{\beta}^\dagger + \hat{\alpha}^\dagger \hat{\beta}), \quad (1)$$

where ω denotes the frequency of uncoupled $\hat{\alpha}$, $\hat{\beta}$ modes and D_r quantifies their mutual coherent coupling, which has its physical origin in the SNC interactions. Without loss of generality, we assume D_r to be real [43,56] noting that its magnitude increases exponentially with the intrinsic squeezing parameter *r* (see Appendix A 1). The eigenmodes of Eq. (1) stem from hybridization between magnon modes $\hat{\alpha}$ and $\hat{\beta}$, and can be conveniently obtained using the antiferromagnetic magnon pseudospin [43]

$$\hat{L}_0 = \frac{1}{2}(\hat{\alpha}^\dagger \hat{\alpha} + \hat{\beta}^\dagger \hat{\beta}), \quad \hat{\mathbf{L}} = \frac{1}{2} \begin{pmatrix} \hat{\alpha} \hat{\beta}^\dagger + \hat{\alpha}^\dagger \hat{\beta} \\ i\hat{\alpha} \hat{\beta}^\dagger - i\hat{\alpha}^\dagger \hat{\beta} \\ \hat{\alpha}^\dagger \hat{\alpha} - \hat{\beta}^\dagger \hat{\beta} \end{pmatrix}, \quad (2)$$

with commutation relations for angular momentum $[\hat{L}_j, \hat{L}_k] = i\epsilon_{jkl}\hat{L}_l$, $j, k, l \in \{x, y, z\}$. With Eq. (2), $\hat{\mathcal{H}}_{\text{Hyb}}$ [Eq. (1)] transforms into $\hat{\mathcal{H}}_{\text{Hyb}} = 2\omega\hat{L}_0 - \omega_0 \cdot \hat{\mathbf{L}}$. The eigenmodes are conveniently obtained via the points where the pseudofield $\omega_0 = 2D_r\hat{\mathbf{e}}_x$ intersects with a unit sphere (Fig. 1) [43], in direct analogy to how electronic spin eigenstates are determined via intersection of the experienced magnetic field with the Bloch sphere.

III. MAGNON PSEUDOSPIN SQUEEZING

To account for quantum fluctuations, we now go beyond the RWA and explicitly account for the counterrotating terms. The total magnonic Hamiltonian then reads [57]

$$\hat{\mathcal{H}}_{\text{AFM}} = \omega(\hat{\alpha}^\dagger \hat{\alpha} + \hat{\beta}^\dagger \hat{\beta}) - D_r(\hat{\alpha} \hat{\beta}^\dagger + \hat{\alpha}^\dagger \hat{\beta}) + D_s(\hat{\alpha}^2 + \hat{\alpha}^{\dagger 2} + \hat{\beta}^2 + \hat{\beta}^{\dagger 2}), \quad (3)$$

with coupling strength D_s stemming from SNC interaction (see Appendix A 1). In the model considered here, we assume D_r and D_s to be independent variables. As detailed in Appendix A 1, D_r and D_s may arise from the same physical interactions and are interrelated in an actual material. On diagonalization, the eigenmodes of $\hat{\mathcal{H}}_{\text{AFM}}$ [Eq. (3)] are annihilated by $\hat{\psi}_\pm$ with the corresponding Fock eigenstates $|m_+, n_-\rangle$. As detailed in Appendix A 2, $|m_+, n_-\rangle$ are related to the magnon Fock states $|m_\alpha, n_\beta\rangle$ —the eigenstates of $\omega(\hat{\alpha}^\dagger \hat{\alpha} + \hat{\beta}^\dagger \hat{\beta})$ —via

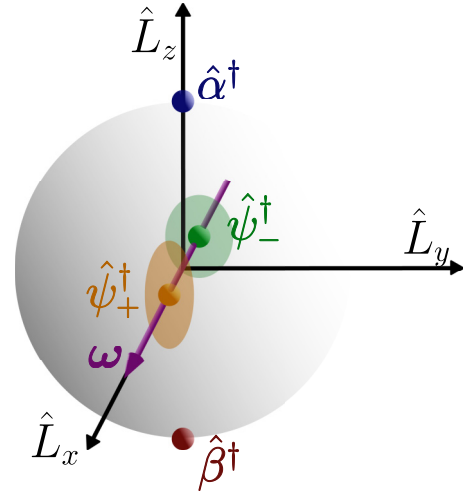


FIG. 1. Representation of the eigenmodes $\hat{\psi}_\pm$ on a unit sphere with uncertainty area of the noncommuting pseudospin components \hat{L}_y and \hat{L}_z . The sphere poles are the pure spin-up and spin-down magnons, represented by creation operators $\hat{\alpha}^\dagger$ and $\hat{\beta}^\dagger$. The considered pseudofield ω is along the \hat{L}_x axis and characterizes spin-0 modes.

a rotation of the pseudofield and two squeeze operations $\hat{S}_\pm(r_\pm)$:

$$|m_+, n_-\rangle = \hat{S}_+(r_+) \hat{S}_-(r_-) \hat{R}_y\left(\frac{\pi}{2}\right) |m_\alpha, n_\beta\rangle, \quad (4)$$

with $\hat{R}_y(\phi) = \exp(-i\phi\hat{L}_y)$, where ϕ is defined as the angle between the *z* axis and pseudofield, $\hat{S}_+(x) = \exp(\frac{x}{2}\hat{R}_y(\frac{\pi}{2}))[\hat{\alpha}^2 - \hat{\alpha}^{\dagger 2}]\hat{R}_y(\frac{\pi}{2})$, where $\hat{S}_-(x)$ is obtained from $\hat{S}_+(x)$ upon substitution $\hat{\alpha} \rightarrow \hat{\beta}$, and quadrature squeeze factors r_\pm ,

$$\tanh(r_\pm) = \frac{2|D_s|}{\omega \mp D_r}, \quad (5)$$

where the ground-state stability requires and ensures $2|D_s| < (\omega - |D_r|)$ and $|D_r| < \omega$.

We find that SNC interactions in $\hat{\mathcal{H}}_{\text{AFM}}$ [Eq. (3)] induce what we term magnon pseudospin squeezing, in system eigenstate $|m_+, n_-\rangle$ [Eq. (4)]. \hat{L}_y and \hat{L}_z are noncommuting $[\hat{L}_y, \hat{L}_z] = i\hat{L}_x$ and therefore obey Heisenberg's uncertainty relation. Considering a special subset of eigenstates where $m \neq 0$ and $n = 0$, as a simpler example, we determine the following expectation value $\langle \hat{L}_x \rangle_{m0}$ and variances $\langle \Delta \hat{L}_i^2 \rangle_{m0} = \langle \hat{L}_i^2 \rangle_{m0} - \langle \hat{L}_i \rangle_{m0}^2$, $i \in y, z$,

$$\langle \hat{L}_x \rangle_{m0} = \frac{m + \frac{1}{2}}{2} \cosh(2r_+) - \frac{\cosh(2r_-)}{4}, \quad (6)$$

$$\langle \Delta \hat{L}_y^2 \rangle_{m0} = \frac{m + \frac{1}{2}}{4} \cosh(2r_+ - 2r_-) - \frac{1}{8}, \quad (7)$$

where $\langle \Delta \hat{L}_z^2 \rangle_{m0}$ can be obtained from $\langle \Delta \hat{L}_y^2 \rangle_{m0}$ [Eq. (7)] upon substitution $-2r_- \rightarrow +2r_-$. We find that the area of uncertainty is given by $\langle \Delta \hat{L}_y^2 \rangle_{m0} \langle \Delta \hat{L}_z^2 \rangle_{m0} = |\langle \hat{L}_x \rangle_{m0}|^2/4 + (m^2 + m)(\cosh 4r_- - 1)/8$ and therefore the state $|m_+, 0_-\rangle$ is not minimum uncertainty since $\langle \Delta \hat{L}_y^2 \rangle_{m0} \langle \Delta \hat{L}_z^2 \rangle_{m0} > |\langle \hat{L}_x \rangle_{m0}|^2/4$. However, the variance in the *y* component fulfils $\langle \Delta \hat{L}_y^2 \rangle_{m0} < |\langle \hat{L}_x \rangle_{m0}|/2$ (see Appendix B) and is hence squeezed.

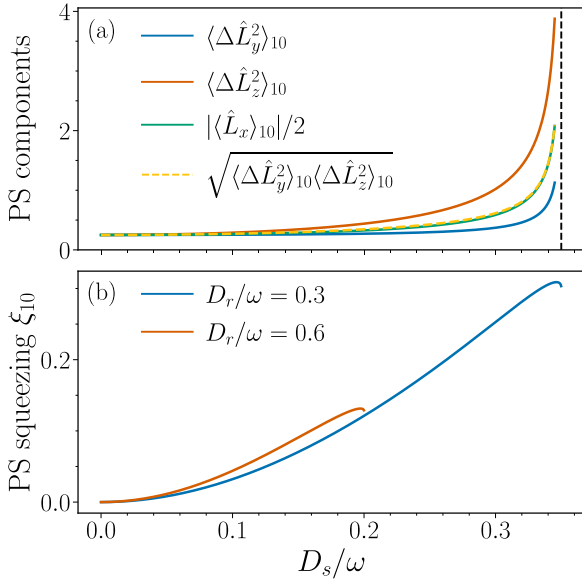


FIG. 2. (a) Expectation value and variances of pseudospin (PS) components $\langle \hat{L}_x \rangle$, $\langle \hat{L}_y^2 \rangle$, and $\langle \hat{L}_z^2 \rangle$ as a function of D_s with $D_r/\omega = 0.3$, $m = 1$, and $n = 0$ [58]. (b) Pseudospin squeezing ξ_{10} as a function of D_s for different values of D_r . The curves are limited by the ground-state stability condition $2|D_s| < (\omega - |D_r|)$ [58].

To quantify squeezing, we define the pseudospin squeezing factor ξ_{m0} by the ellipticity of quantum fluctuations in the \hat{L}_y - \hat{L}_z plane [2], which is explicitly given by

$$\xi_{m0} = -\frac{1}{4} \ln \left(\frac{\langle \hat{L}_y^2 \rangle_{m0}}{\langle \hat{L}_z^2 \rangle_{m0}} \right). \quad (8)$$

In the schematics of Fig. 1, we qualitatively sketch the eigenmodes $\hat{\psi}_{\pm}$ on the Bloch sphere with the corresponding squeezed uncertainty regions in the \hat{L}_y - \hat{L}_z plane. In Fig. 2(a) we plot expectation value and variances of pseudospin components $\langle \hat{L}_x \rangle_{10}$, $\langle \hat{L}_y^2 \rangle_{10}$, and $\langle \hat{L}_z^2 \rangle_{10}$ as a function of D_s , demonstrating that $\langle \hat{L}_y^2 \rangle_{10} < |\langle \hat{L}_x \rangle_{10}|/2$. In Fig. 2(b), we plot pseudospin squeezing ξ_{10} [Eq. (2)] as a function of D_s for two values of D_r showing that ξ_{10} is a steadily growing function of D_s , i.e., $\xi_{10} = 0$ if $D_s = 0$. Therefore, D_s is responsible for pseudospin squeezing. At the instability, where $2|D_s| = (\omega - |D_r|)$, pseudospin squeezing approaches $\xi_{10} \rightarrow r_-$ (see Appendix B). For completeness, we furthermore comment that we assume a temperature of $T = 0$ K in the model considered here. The equilibrium squeezing here is amplified by strong exchange interactions. If the local dissipation rate is small in comparison to the coupling strength of the internal interaction causing squeezing, its effect is expected to be small [59]. A detailed discussion of the effect of finite temperature is left for future work.

IV. PSEUDOSPIN SQUEEZING IN THE GROUND STATE

In this subsection, we discuss the special case of pseudospin squeezing in the ground state since it differs qualitatively from the previously known case of spin squeezing in its ground state $|0_+, 0_- \rangle$ [Eq. (A26)]. Considering $m = 0$ and $n = 0$ for pseudospin squeezing ξ_{m0} [Eq. (B14)], we can

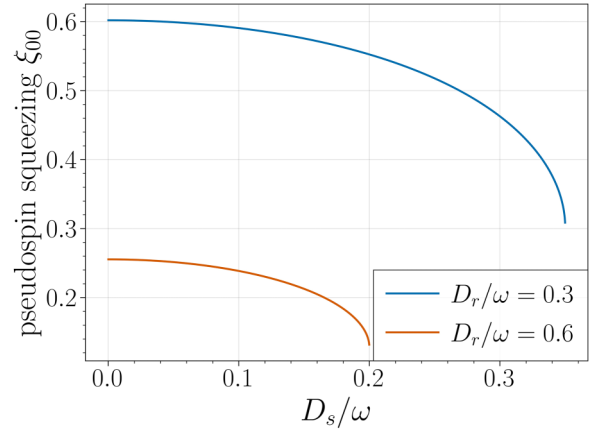


FIG. 3. Plot of pseudospin squeezing ξ_{00} in the ground state $|0, 0 \rangle$ as a function of D_s [58].

already see that ξ_{00} is decreasing with increasing D_s . This is unconventional since D_s is what is causing squeezing. The limit $D_s \rightarrow 0$ therefore has to be treated carefully in case of the ground state. One reason is that the operator $\hat{L}^2 = (\hat{N}/2)(\hat{N}/2 + 1)$ [60], with the number operator $\hat{N} = \hat{\alpha}^\dagger \hat{\alpha} + \hat{\beta}^\dagger \hat{\beta}$ has a vanishing expectation value for the magnon vacuum. Hence, in the case where we consider the ground state and the coupling $D_s = 0$, the magnitude of pseudospin $\langle \hat{L}^2 \rangle_{00}$ vanishes. Therefore, our Bloch sphere has zero radius and our basis is ill-defined. This is the difference between electron spin, where S is always finite, and bosonic pseudospin.

Let us carefully evaluate the limit $D_s \rightarrow 0$ by expanding Eqs. (6)–(B9) for $m = 0$ in the small $|D_s| \ll (\omega - D_r)/2$ limit. We find

$$\langle \hat{L}_x \rangle_{00} \approx \frac{1}{2} \left(\frac{1}{(\omega - D_r)^2} - \frac{1}{(\omega + D_r)^2} \right) |D_s|^2, \quad (9)$$

$$\langle \hat{L}_y^2 \rangle_{00} \approx \frac{1}{4} \left(\frac{1}{\omega - D_r} - \frac{1}{\omega + D_r} \right)^2 |D_s|^2, \quad (10)$$

$$\langle \hat{L}_z^2 \rangle_{00} \approx \frac{1}{4} \left(\frac{1}{\omega - D_r} + \frac{1}{\omega + D_r} \right)^2 |D_s|^2. \quad (11)$$

It follows that ξ_{00} in the small $|D_s| \ll (\omega - D_r)/2$ limit has a finite value

$$\xi_{00} \approx \frac{1}{2} \ln \left(\frac{\omega}{D_r} \right). \quad (12)$$

However, the $D_s = 0$ limit is ill defined since $\langle \hat{L}_x \rangle_{00} = \langle \hat{L}_y^2 \rangle_{00} = \langle \hat{L}_z^2 \rangle_{00} = 0$. This is because it requires the presence of a nonzero $D_s \neq 0$ to break symmetry and therefore induce squeezing. The intrasublattice coupling D_s is hence causing squeezing but demonstrates unconventional behavior in the ground state $|0_+, 0_- \rangle$ [Eq. (A26)]. In Fig. 3, the ground state squeezing ξ_{00} is plotted as a function of D_s for several values of D_r .

V. COUPLING ENHANCEMENT

Exponentially enhanced coupling between a squeezed bosonic mode and another quasiparticle has been demonstrated theoretically and experimentally in a wide range of

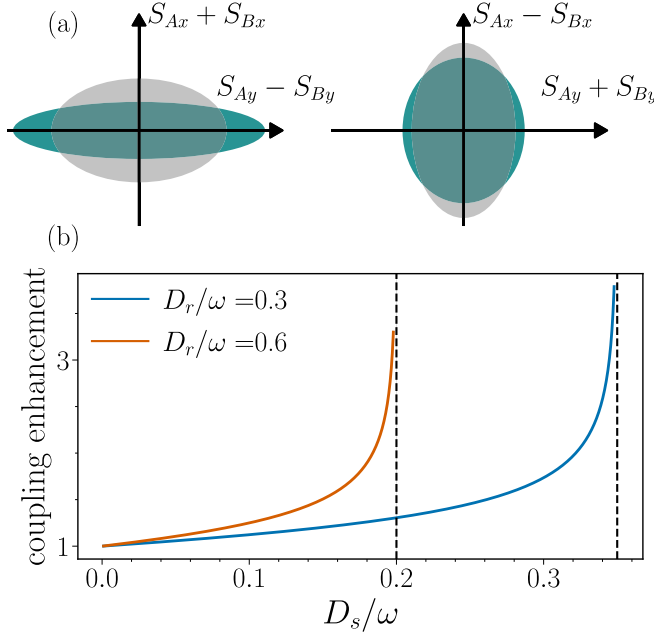


FIG. 4. (a) Uncertainty region of the quadratures $\hat{X}_{1/2}$ and $\hat{Y}_{1/2}$ of sublattice spin operators $\hat{S}_{A/B}$ for an AFM with $D_s \approx 0$ (gray) and AFM with SNC interactions (green). (b) Coupling enhancement $\cosh(r + r_+)/\cosh r$ of $\hat{\psi}_+$ in the ground state $|0_+, 0_- \rangle$ for an uncompensated interface as a function of D_s , with intrinsic squeezing $r = 1$ [58].

systems [2–4]. Equilibrium squeezing inherits this property and enables enhanced coupling between, for example, itinerant electrons of normal metals and AFM magnons [28] when the interaction is mediated by sublattice spin [28,61–63]. We now employ this principle in demonstrating an additional enhancement and control of coupling between an antiferromagnetic magnonic mode and itinerant electrons, using them as an example, via the magnon pseudospin squeezing.

Let us denote sublattice spin operators \hat{S}_A and \hat{S}_B where A (B) signifies the spin-down (up) sublattice and define the four quadrature operators $\hat{X}_{1/2} = (\hat{S}_{Ax/y} + \hat{S}_{Bx/y})/\sqrt{4NS}$ and $\hat{Y}_{1/2} = (-\hat{S}_{Ay/x} + \hat{S}_{By/x})/\sqrt{4NS}$. Here, N denotes the number of sublattice sites and S the spin of a single lattice site. In an AFM with negligible quadratic interactions ($D_s \approx 0$), the ground-state fluctuations of quadrature operator $\hat{X}_{1/2}$ (sum of sublattice spins) is reduced in comparison to the variance of $\hat{Y}_{1/2}$ (difference of sublattice spins) because of intrinsic squeezing [see Fig. 4(a)]. The sublattice spins prefer to stay antiparallel, therefore forming correlations [28,29]. In the eigenmodes harboring magnon pseudospin squeezing evaluated above, we find that the variances of the quadrature operators $\hat{X}_{1/2}$ and $\hat{Y}_{1/2}$ in the ground state $|0_+, 0_- \rangle$ [Eq. (4)] read

$$\langle \Delta \hat{X}_{1/2}^2 \rangle_{00} = \frac{e^{-2(r \pm r_{\pm})}}{4}, \quad \langle \Delta \hat{Y}_{1/2}^2 \rangle_{00} = \frac{e^{2(r \pm r_{\pm})}}{4}. \quad (13)$$

In comparison with an AFM with $D_s \approx 0$, where $\langle \Delta \hat{X}_1^2 \rangle_{00} = \langle \Delta \hat{X}_2^2 \rangle_{00}$ and $\langle \Delta \hat{Y}_1^2 \rangle_{00} = \langle \Delta \hat{Y}_2^2 \rangle_{00}$ [29], we find that SNC interactions quadratic in magnon operators $\hat{\alpha}$ and $\hat{\beta}$ cause an asymmetry between the x and y components of spin operators,

as illustrated in the schematics of Fig. 4(a). This introduces a new way of engineering quantum fluctuations in AFMs.

Focusing on a concrete example of AFM interfaces with a normal metal, we consider interaction between electrons and the AFM modes via interfacial exchange coupling between sublattice spins and electron spin [28,64,65]:

$$\hat{H}_{\text{NA}} = \sum_{\mathbf{q}_1, \mathbf{q}_2} \hat{c}_{\mathbf{q}_1 \uparrow}^\dagger \hat{c}_{\mathbf{q}_2 \downarrow} [(W_{\mathbf{q}_1 \mathbf{q}_2}^A \cosh r - W_{\mathbf{q}_1 \mathbf{q}_2}^B \sinh r) \hat{\alpha} + (W_{\mathbf{q}_1 \mathbf{q}_2}^B \cosh r - W_{\mathbf{q}_1 \mathbf{q}_2}^A \sinh r) \hat{\beta}^\dagger] + \text{H.c.}, \quad (14)$$

where $\hat{c}_{q\sigma}$ denotes the annihilation operator of an electron with momentum \mathbf{q} and spin σ and $W_{\mathbf{q}_1 \mathbf{q}_2}^{A/B}$ the scattering amplitude, which includes information about the interfacial coupling strength with sublattice A and B , respectively. In the eigenbasis $\hat{\psi}_\pm$, the scattering Hamiltonian \hat{H}_{NA} [Eq. (14)] reads

$$\hat{H}_{\text{NA}} = \sum_{\mathbf{q}_1, \mathbf{q}_2, \gamma = \pm} \hat{c}_{\mathbf{q}_1 \uparrow}^\dagger \hat{c}_{\mathbf{q}_2 \downarrow} (s_\gamma U_\gamma \hat{\psi}_\gamma + V_\gamma \hat{\psi}_\gamma^\dagger) + \text{H.c.}, \quad (15)$$

with $s_\pm = \pm 1$ and amplitudes

$$U_\pm = W_{\mathbf{q}_1 \mathbf{q}_2}^A \frac{\cosh(r \pm r_\pm)}{\sqrt{2}} - W_{\mathbf{q}_1 \mathbf{q}_2}^B \frac{\sinh(r \pm r_\pm)}{\sqrt{2}}, \quad (16)$$

where $V_+(V_-)$ can be obtained from $U_+(U_-)$ upon exchange $W_{\mathbf{q}_1 \mathbf{q}_2}^A \leftrightarrow W_{\mathbf{q}_1 \mathbf{q}_2}^B$. We find that for a compensated interface ($W_{\mathbf{q}_1 \mathbf{q}_2}^A = W_{\mathbf{q}_1 \mathbf{q}_2}^B$) the scattering amplitudes [Eq. (16)] are exponentially suppressed by $e^{-(r+r_+)}$ and $e^{-(r-r_-)}$, whereas for an uncompensated interface with $W_{\mathbf{q}_1 \mathbf{q}_2}^A = 0$ and $W_{\mathbf{q}_1 \mathbf{q}_2}^B \neq 0$ the creation of the $\hat{\psi}_+^\dagger$ mode is enhanced by $\cosh(r + r_+)$. This feature allows for mode selection and modification of scattering amplitudes by tuning the parameters D_r and D_s . In Fig. 4(b) we plot the coupling enhancement $\cosh(r + r_+)$ as a function of D_s and normalized to the coupling enhancement of an AFM with $D_s \approx 0$ given by $\cosh r$.

VI. QUANTUM CONTROL AND SUPERPOSITION RESOLUTION VIA A QUBIT

A hallmark of squeezed states is that they are comprised by quantum superpositions that underlie nearly all their unique properties. Experimentally detecting these intrinsic superpositions should offer direct access to their quantum features. Recent theoretical proposals suggest a direct dispersive interaction between spin qubits and magnets for probing these superpositions in the ground state via qubit spectroscopy [66,67]. Here, we show that this interaction enables a qubit-state dependent pseudofield thereby enabling a quantum control of the AFM ground state and eigenmodes [see Fig. 5(a)].

We consider direct dispersive coupling between a spin qubit and AFM with a compensated interface, described by the following interaction Hamiltonian [67]

$$\hat{H}_{\text{qcon}} = \chi (\hat{\alpha}^\dagger \hat{\alpha} - \hat{\beta}^\dagger \hat{\beta}) \hat{\sigma}_z = 2\chi \hat{L}_z \hat{\sigma}_z, \quad (17)$$

with the interaction strength χ ; see Appendix C 1 for the derivation of \hat{H}_{qcon} [Eq. (17)]. The Hamiltonian representing the coupled magnet-qubit system reads $\hat{H}_{\text{mq}} = \hat{H}_{\text{AFM}} + \hat{H}_{\text{q}} + \hat{H}_{\text{qcon}}$, where $\hat{H}_{\text{q}} = \omega_q \hat{\sigma}_z/2$ stands for the spin qubit

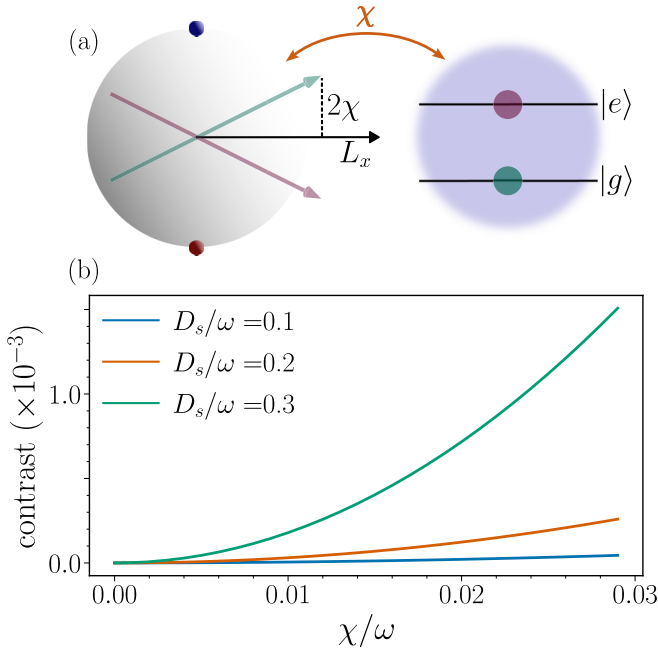


FIG. 5. (a) Control of pseudofield via qubit in the ground state $|g\rangle$ (green) and excited state $|e\rangle$ (pink). (b) Contrast of the nontrivial peak in the small $\chi/D_r \ll 1$ approximation as a function of χ with $D_r/\omega = 0.3$ for three values of D_s .

with level splitting ω_q . To evaluate the effect of the qubit on the pseudospin state, we consider the reduced Hamiltonians $\hat{\mathcal{H}}_g = \langle g | \hat{\mathcal{H}}_{\text{mq}} | g \rangle$ and $\hat{\mathcal{H}}_e = \langle e | \hat{\mathcal{H}}_{\text{mq}} | e \rangle$, where $|g\rangle$ ($|e\rangle$) denotes the qubit ground (excited) state.

The eigenstates of $\hat{\mathcal{H}}_{g/e}$, denoted by $|m, n\rangle_{g/e}$, are obtained from Eqs. (4) and (5) upon substitution $D_r \rightarrow \sqrt{D_r^2 + \chi^2}$ and $\pi/2 \rightarrow \theta_{g/e}$ where we defined angles $\theta_{g/e} = \pi/2 \mp \tilde{\theta}$ with $\sin \tilde{\theta} = 1/\sqrt{1 + D_r^2/\chi^2}$ [68]. Consequently, the pseudofield is modified by the qubit as $\omega_{g/e} = \omega_0 \pm 2\chi \hat{e}_z$ (see Appendix C 2), which is illustrated in the schematics of Fig. 5(a). We find that pseudospin squeezing of states $|m, n\rangle_g$ ($|m, n\rangle_e$) can be defined for the rotated pseudospin components $\hat{J}_i^{g/e} = R_y(\theta_{g/e}) \hat{L}_i R_y^\dagger(\theta_{g/e})$. The corresponding squeeze factor $\xi_{m0}^g = \xi_{m0}^e \equiv \xi_{m0}^\chi$ can be obtained from Eq. (8) upon substitution $D_r \rightarrow \sqrt{D_r^2 + \chi^2}$. For small $\chi/D_r \ll 1$, we find $\xi_{m0}^\chi \approx \xi_{m0} + c_2 \chi^2$ [69]. Thus, the magnon pseudospin state, eigenmodes, and fluctuations can be modified in a controlled way via the coupling strength χ and the state of the qubit.

Finally, the ground state $|0, 0\rangle_g$ can be expressed in terms of a quantum superposition of multiple excited states $|m, n\rangle_e$. This composition, for small $\chi/D_r \ll 1$, is obtained as

$$|0, 0\rangle_g \approx |0, 0\rangle_e - \chi \frac{\sinh(r_+ - r_-)}{2D_r} |1, 1\rangle_e. \quad (18)$$

Because of the nonvanishing overlap $\langle 1, 1 | 0, 0 \rangle_g \neq 0$, the qubit can be excited into the state $|1, 1\rangle_e$ when it is driven at frequency ω_{11} —the energy difference between $|0, 0\rangle_g$ and $|1, 1\rangle_e$ —with a probability of $c = |\langle 1, 1 | 0, 0 \rangle_g|^2$ (see Appendix C 3). Driving the qubit over a range of frequencies and measuring its steady state excitation reveals a nontrivial peak around ω_{11} with a height proportional to the exci-

tation probability c , which we label as the contrast. This nontrivial signature stems from pseudospin squeezing and can be used to resolve the ground-state quantum superposition via the described qubit spectroscopy [66]. In Fig. 5(b) we plot contrast c as a function of χ in the small χ limit.

VII. DISCUSSION AND CONCLUSIONS

Antiferromagnets as a platform hosting interacting bosonic modes offer a convenient tunability of the system parameters ω , r , D_r , and D_s via external magnetic fields and shape anisotropy [70–72]. However, our results are applicable to other bosonic systems and theoretically introduce quantum engineering of bosonic pseudospin and its fluctuations. We clarify that our work here focuses on *equilibrium* squeezing which is promising as a resource for quantum computational purposes.

As detailed in Appendix A 1 and D, the easy-plane AFMs nickel oxide and hematite above Morin temperature can be described by a Hamiltonian in the form of $\hat{\mathcal{H}}_{\text{AFM}}$ [Eq. (3)] and hence realize the model presented here. However, a similar effective Hamiltonian can be achieved for easy-axis AFMs in the spin-flop and the canted phase [57]. While the intra-sublattice interactions responsible for the magnon pseudospin squeezing are typically weaker than exchange and are often neglected, the coupling strengths D_r and D_s are greatly enhanced by intrinsic squeezing $\propto \sinh(2r)$ and $\propto \cosh(2r)$, respectively (see Appendix A 1), making the magnon pseudospin squeezing a large effect. In the case of nickel oxide, the coupling strengths are estimated to be $D_r/\omega \approx 0.48$ and $D_s/\omega \approx 0.24$. Thus, the relatively large values of D_r and D_s evaluated here highlight the importance of taking SNC interactions into account (see Appendix A 1). Furthermore, the model we study here can be used to describe recently realized qubit-magnon platforms, such as the antiferromagnetic van der Waals magnet CrSBr with a defect acting as a spin qubit [52,53]. Furthermore, as discussed in Refs. [66,67], semiconducting quantum dots coupled to magnets via interfacial exchange interaction realize the required interaction and sufficiently large coupling strength for quantum control.

Considering atomic ensembles as an example, spin squeezing has been mathematically proposed as an entanglement test for bosons [60]. Here, we present a concrete platform exhibiting the spin squeezing [60] along with a method of probing squeezing via qubit spectroscopy. Moreover, this platform provides squeezed Fock states [73,74] which have recently been proposed as a resource for quantum error correction [75]. Because of this and the possibility of state control via a qubit, our analysis highlights new opportunities for quantum technologies. At the same time, the spin-nonconserving interactions and the concomitant magnon pseudospin squeezing introduce a knob to tune and engineer quantum fluctuations, coupling to electrons and mode selection expected to be useful in designing spintronic devices [72,76–78]. Furthermore, antiferromagnets with a three-sublattice groundstate configuration [79,80] offer a third degree of freedom which may address qutrits more effectively, motivating to study these types of platforms in the future.

ACKNOWLEDGMENTS

This work was funded by the Spanish Ministry of Science, Innovation and Universities-Agencia Estatal de Investigación through the Grants No. PID2021-125894NB-I00 and No. CEX2023-001316-M (through the “María de Maeztu” program for Units of Excellence in R&D). A.-L.E.R. acknowledges that the project that gave rise to these results received the support of a fellowship from “la Caixa” Foundation (ID No. 100010434) with the Fellowship Code No. LCF/BQ/DI22/11940029. A.K. was supported by the Spanish Ministry for Science and Innovation—AEI Grant No. RYC2021 031063-I, and the German Research Foundation (DFG) via Spin + X TRR 173-268565370, Project No. A13. F.J.G.-V. also thanks the support from the “(MAD2D-CM)-UAM7” project funded by Comunidad de Madrid, by the Recovery, Transformation, and Resilience Plan, and by NextGenerationEU from the European Union.

DATA AVAILABILITY

The data that support the findings of this article are openly available [58].

APPENDIX A: DERIVATION AND DIAGONALIZATION OF THE HAMILTONIAN

In this Appendix, we want to derive the Hamiltonian used in the main text $\hat{\mathcal{H}}_{\text{AFM}}$ [Eq. (4)] from a spin model and then proceed to diagonalize it. In Appendix A 1, we perform the derivation of the system Hamiltonian $\hat{\mathcal{H}}_{\text{AFM}}$ [Eq. (4)] for the easy-plane antiferromagnet (AFM) nickel oxide and discuss the origin of coupling strengths D_r and D_s . In Appendix A 2, we proceed by diagonalizing $\hat{\mathcal{H}}_{\text{AFM}}$ making use of the pseudospin formalism and discussing the transformations and operators involved in the diagonalization.

1. Spin Hamiltonian of easy-plane antiferromagnet

Here, we derive the Hamiltonian $\hat{\mathcal{H}}_{\text{AFM}}$ [Eq. (4) in the main text] from a spin model for the easy-plane AFM Nickel Oxide (NiO). We start from classical ground state of an AFM, called Néel state, that consists of two fully and oppositely polarized sublattices below the Néel temperature. NiO has a hard-axis and easy-axis anisotropy. The hard-axis anisotropy is along the $\langle 111 \rangle$ axis and forces the spins into the $\{111\}$ planes [57,81]. The easy-axis anisotropy is along the $\langle 11\bar{2} \rangle$ axes. There are three equivalent $\langle 11\bar{2} \rangle$ directions in the $\{111\}$ planes [57]. Here, we denote the spin-down (up) sublattice as A (B). Following Refs. [57,81,82], we start with the Hamiltonian describing a bipartite lattice AFM with easy-plane anisotropy and applied magnetic field ($\hbar = 1$),

$$\begin{aligned} \mathcal{H}_{\text{NiO}} = & |\gamma| H_0 \sum_{i \in A, j \in B} (\hat{S}_i^z + \hat{S}_j^z) + 2J \sum_{(i,j)} \hat{\mathbf{S}}_i \cdot \hat{\mathbf{S}}_j \\ & + K_x \sum_{i \in A, j \in B} [(\hat{S}_i^x)^2 + (\hat{S}_j^x)^2] \\ & - K_z \sum_{i \in A, j \in B} [(\hat{S}_i^z)^2 + (\hat{S}_j^z)^2], \end{aligned} \quad (\text{A1})$$

with $\hat{S}_{i/j}^\pm = \hat{S}_{i/j}^x \pm i\hat{S}_{i/j}^y$, the gyromagnetic ratio $\gamma < 0$, J denoting the exchange interaction of nearest neighbors belonging to different sublattices, the easy-plane anisotropy K_x and easy-axis anisotropy K_z . Here, z' denotes one of the easy directions along the $\langle 11\bar{2} \rangle$ axes. We also consider an applied magnetic field along one of the z' directions, denoted by $\mathbf{H} = H_0 \hat{e}_{z'}$. Note here that the index i (j) marks lattice sites belonging to sublattice A (B).

To quantize our Hamiltonian $\hat{\mathcal{H}}_{\text{NiO}}$ [Eq. (A1)], we use the following linearized Holstein-Primakoff (HP) transformations for lattice sites $i \in A$ and $j \in B$ [57,83]

$$\begin{aligned} \hat{S}_i^+ &= \sqrt{\frac{2S}{N}} \sum_{\mathbf{k}} e^{-i\mathbf{k} \cdot \mathbf{r}_i} \hat{a}_{\mathbf{k}}^\dagger, & \hat{S}_j^+ &= \sqrt{\frac{2S}{N}} \sum_{\mathbf{k}} e^{i\mathbf{k} \cdot \mathbf{r}_j} \hat{b}_{\mathbf{k}}, \\ \hat{S}_i^- &= \sqrt{\frac{2S}{N}} \sum_{\mathbf{k}} e^{i\mathbf{k} \cdot \mathbf{r}_i} \hat{a}_{\mathbf{k}}, & \hat{S}_j^- &= \sqrt{\frac{2S}{N}} \sum_{\mathbf{k}} e^{-i\mathbf{k} \cdot \mathbf{r}_j} \hat{b}_{\mathbf{k}}^\dagger, \\ \hat{S}_i^z &= -S + \frac{1}{N} \sum_{\mathbf{k}, \mathbf{k}'} e^{-i(\mathbf{k}-\mathbf{k}') \cdot \mathbf{r}_i} \hat{a}_{\mathbf{k}}^\dagger \hat{a}_{\mathbf{k}'}, \\ \hat{S}_j^z &= S - \frac{1}{N} \sum_{\mathbf{k}, \mathbf{k}'} e^{-i(\mathbf{k}-\mathbf{k}') \cdot \mathbf{r}_j} \hat{b}_{\mathbf{k}}^\dagger \hat{b}_{\mathbf{k}'}, \end{aligned} \quad (\text{A2})$$

where S denotes the individual total spin of each lattice site and N the number of sublattice spins. The quantization axes are different for the two sublattice because of their opposite spin orientation. The operators $\hat{a}_{\mathbf{k}}$ ($\hat{b}_{\mathbf{k}}$) represent the annihilation operator of a spin-up (down) excitation on sublattice A (B). They fulfill the bosonic commutation relations $[\hat{a}_{\mathbf{k}}, \hat{a}_{\mathbf{k}'}^\dagger] = \delta_{\mathbf{k}\mathbf{k}'}$, $[\hat{b}_{\mathbf{k}}, \hat{b}_{\mathbf{k}'}^\dagger] = \delta_{\mathbf{k}\mathbf{k}'}$, and $[\hat{a}_{\mathbf{k}}, \hat{b}_{\mathbf{k}'}^\dagger] = 0$ and will be denoted spin-up (down) sublattice magnons $\hat{a}_{\mathbf{k}}$ ($\hat{b}_{\mathbf{k}}$). Note that the linearized HP transformations are only valid if the average number of excitations is small in comparison with the spin at each lattice site S . Using the linear HP transformations [Eq. (A2)], we arrive at the Hamiltonian

$$\begin{aligned} \hat{\mathcal{H}}_{\text{NiO}} = & \sum_{\mathbf{k}} \frac{A}{2} \hat{a}_{\mathbf{k}}^\dagger \hat{a}_{\mathbf{k}} + \frac{B}{2} \hat{b}_{\mathbf{k}}^\dagger \hat{b}_{\mathbf{k}} + C_{\mathbf{k}} \hat{a}_{\mathbf{k}} \hat{b}_{-\mathbf{k}} \\ & + D(\hat{a}_{\mathbf{k}} \hat{a}_{-\mathbf{k}} + \hat{b}_{\mathbf{k}} \hat{b}_{-\mathbf{k}}) + \text{H.c.}, \end{aligned} \quad (\text{A3})$$

with

$$\begin{aligned} A &= |\gamma| \left(H_E + \frac{H_{Ax}}{2} + H_{Az} + H_0 \right), \\ B &= |\gamma| \left(H_E + \frac{H_{Ax}}{2} + H_{Az} - H_0 \right), \\ C_{\mathbf{k}} &= |\gamma| \gamma_{\mathbf{k}} H_E, \quad D = |\gamma| \frac{H_{Ax}}{4}, \end{aligned} \quad (\text{A4})$$

and $H_E = 2S_z J / |\gamma|$, $H_{Ax} = 2SK_x / |\gamma|$, $H_{Az} = 2SK_z / |\gamma|$, and $\gamma_{\mathbf{k}} = \cos(a|\mathbf{k}|/2)$. Here, z is the number of nearest neighbors and a the lattice constant of NiO.

Considering a nanomagnet where the $\mathbf{k} \neq \mathbf{0}$ modes are well separated from the Kittel mode $\mathbf{k} = \mathbf{0}$ [84], we focus on the homogeneous mode $\mathbf{k} = \mathbf{0}$ here. We can therefore drop the index \mathbf{k} in the operators and coefficients and define $\hat{a} \equiv \hat{a}_{\mathbf{0}}$, $\hat{b} \equiv \hat{b}_{\mathbf{0}}$, and $C \equiv C_{\mathbf{0}}$, where $\gamma_0 = 1$. Additionally assuming $H_0 = 0$, such that $A = B$ [Eq. (A4)], our Hamiltonian \mathcal{H}_{NiO}

[Eq. (A3)] becomes

$$\begin{aligned}\hat{\mathcal{H}}_{\text{NiO}} = & A\hat{a}^\dagger\hat{a} + B\hat{b}^\dagger\hat{b} + C(\hat{a}\hat{b} + \hat{a}^\dagger\hat{b}^\dagger) \\ & + D(\hat{a}^2 + \hat{b}^2 + \hat{a}^{\dagger 2} + \hat{b}^{\dagger 2}).\end{aligned}\quad (\text{A5})$$

where, for now, we assume the parameters A , C , and D to be real. We define spin-up and spin-down magnon operators $\hat{\alpha}$ and $\hat{\beta}$ via the two-mode Bogoliubov transformation [28]

$$\begin{pmatrix} \hat{\alpha} \\ \hat{\beta}^\dagger \end{pmatrix} = \begin{pmatrix} u & v \\ v & u \end{pmatrix} \begin{pmatrix} \hat{a} \\ \hat{b}^\dagger \end{pmatrix}, \quad (\text{A6})$$

with the coefficients

$$u = \frac{1}{\sqrt{2}}\sqrt{\frac{A}{\omega} + 1}, \quad v = \frac{1}{\sqrt{2}}\sqrt{\frac{A}{\omega} - 1}, \quad (\text{A7})$$

and the energy $\omega = \sqrt{A^2 - C^2}$. The Bogoliubov coefficients u and v [Eq. (A7)] define intrinsic two-mode squeezing r by $\tanh(r) = v/u$. This squeezing stems from the strong inter-sublattice exchange interaction and is typically large in AFMs. Magnons, represented by $\hat{\alpha}$ and $\hat{\beta}$, are therefore intrinsically squeezed. In the new basis [Eq. (A6)], the Hamiltonian $\hat{\mathcal{H}}_{\text{NiO}}$ [Eq. (A5)] reads

$$\begin{aligned}\hat{\mathcal{H}}_{\text{AFM}} = & \omega(\hat{\alpha}^\dagger\hat{\alpha} + \hat{\beta}^\dagger\hat{\beta}) - D_r(\hat{\alpha}\hat{\beta}^\dagger + \hat{\alpha}^\dagger\hat{\beta}) \\ & + D_s(\hat{\alpha}^2 + \hat{\alpha}^{\dagger 2} + \hat{\beta}^2 + \hat{\beta}^{\dagger 2}) + (\omega - A),\end{aligned}\quad (\text{A8})$$

where we defined $D_r = 2D \sinh(2r)$ and $D_s = D \cosh(2r)$. Hence, in the platform considered here, D_r and D_s are not independent variables. The form of the antiferromagnetic Hamiltonian [Eq. (A8)] is the form we used in the main text which is why we denote the Hamiltonian by $\hat{\mathcal{H}}_{\text{AFM}}$ from now on. We show in the following subsection that the parameter D_r causes a hybridization of modes $\hat{\alpha}$ and $\hat{\beta}$ and hence a *rotation* of pseudospin on the Bloch sphere whereas D_s induces *squeezing* of the hybridized modes and hence the pseudospin components. Finally, using the following effective values $H_E = 9684$ kOe, $H_{Ax} = 6.35$ kOe, $H_{Az} = 0.11$ kOe [57], and $H_0 = 0$, we find the coefficients $A = B = |\gamma| \cdot 9687.285$ kOe, $C = |\gamma| \cdot 9684$ kOe, and $D = |\gamma| \cdot 1.5875$ kOe. Therefore, D is four orders of magnitude smaller than typical values of A , B , and C , thereby motivating why it has often been disregarded in previous studies. However, D_r and D_s are enhanced by intrinsic squeezing r . We estimate $\omega \approx |\gamma| \cdot 252.26$ kOe = $2\pi \cdot 0.7$ THz, $r \approx 2.17$, $D_r/\omega \approx 0.48$, and $D_s/\omega \approx 0.24$.

2. Eigenstates of the bare antiferromagnet

In this subsection, we diagonalize the Hamiltonian $\hat{\mathcal{H}}_{\text{AFM}}$ [Eq. (A8)] via the pseudospin formalism [43,60] and a one-mode squeeze transformation. We start from a reduced Hamiltonian, setting $D_s = 0$ in $\hat{\mathcal{H}}_{\text{AFM}}$ [Eq. (A8)], which results in

$$\hat{\mathcal{H}}_{\text{hyb}} = \omega(\hat{\alpha}^\dagger\hat{\alpha} + \hat{\beta}^\dagger\hat{\beta}) - D_r(\hat{\alpha}\hat{\beta}^\dagger + \hat{\alpha}^\dagger\hat{\beta}). \quad (\text{A9})$$

The coherent coupling between the spin-up and spin-down magnon $\hat{\alpha}$ and $\hat{\beta}$ proportional to $\propto D_r$ leads to a hybridization of magnons.

As the next step, we introduce the symmetric and antisymmetric modes $\hat{\psi}_s$ and $\hat{\psi}_a$ as

$$\hat{\psi}_s = \frac{1}{\sqrt{2}}(\hat{\alpha} + \hat{\beta}), \quad \hat{\psi}_a = \frac{1}{\sqrt{2}}(-\hat{\alpha} + \hat{\beta}), \quad (\text{A10})$$

which diagonalize $\hat{\mathcal{H}}_{\text{hyb}}$ [Eq. (A9)] as

$$\hat{\mathcal{H}} = \omega_s \hat{\psi}_s^\dagger \hat{\psi}_s + \omega_a \hat{\psi}_a^\dagger \hat{\psi}_a + (\omega - A), \quad (\text{A11})$$

with the energies

$$\omega_s = \omega - D_r, \quad \omega_a = \omega + D_r. \quad (\text{A12})$$

The symmetric and antisymmetric modes $\hat{\psi}_s$ and $\hat{\psi}_a$ [Eq. (A10)] correspond to maximal hybridization of the magnons $\hat{\alpha}$ and $\hat{\beta}$. This is because magnons $\hat{\alpha}$ and $\hat{\beta}$ are degenerate here. The eigenmodes of $\hat{\mathcal{H}}_{\text{hyb}}$ can also be treated within a pseudospin framework defining the pseudospin components [43]

$$\hat{L}_0 = \frac{1}{2}(\hat{\alpha}^\dagger\hat{\alpha} + \hat{\beta}^\dagger\hat{\beta}), \quad \hat{\mathbf{L}} = \frac{1}{2} \begin{pmatrix} \hat{\alpha}\hat{\beta}^\dagger + \hat{\alpha}^\dagger\hat{\beta} \\ i\hat{\alpha}\hat{\beta}^\dagger - i\hat{\alpha}^\dagger\hat{\beta} \\ \hat{\alpha}^\dagger\hat{\alpha} - \hat{\beta}^\dagger\hat{\beta} \end{pmatrix}. \quad (\text{A13})$$

The Hamiltonian $\hat{\mathcal{H}}_{\text{hyb}}$ can be reformulated using pseudospin operators \hat{L}_i , $i \in \{0, 1, 2, 3\}$ as

$$\hat{\mathcal{H}}_{\text{hyb}} = 2\omega\hat{L}_0 - \boldsymbol{\omega}^0 \cdot \hat{\mathbf{L}} + (\omega - A), \quad (\text{A14})$$

with pseudofield $\boldsymbol{\omega}^0 = 2D_r\hat{\mathbf{e}}_x$. In the pseudospin framework, we can picture the eigenmodes on a Bloch unit sphere, where the poles correspond to the $\hat{\alpha}$ and $\hat{\beta}$ magnons. The hybridized modes are then characterized by the pseudofield $\boldsymbol{\omega}^0$ and correspond to the intersection of the pseudofield with the Bloch sphere. The eigenmodes $\hat{\psi}_s$ and $\hat{\psi}_a$ can be obtained from the following transformation [43]:

$$\begin{pmatrix} \hat{\psi}_s \\ \hat{\psi}_a \end{pmatrix} = \begin{pmatrix} \cos(\frac{\theta}{2}) & \sin(\frac{\theta}{2}) \\ -\sin(\frac{\theta}{2}) & \cos(\frac{\theta}{2}) \end{pmatrix} \begin{pmatrix} \hat{\alpha} \\ \hat{\beta} \end{pmatrix}, \quad (\text{A15})$$

with the rotation angle $\cos\theta = \omega_z^0/|\boldsymbol{\omega}^0|$. Here, this angle is $\theta = \pi/2$. Finally, the transformation Eq. (A15) can be expressed via a rotation operator

$$\hat{R}_y(\theta) = \exp(-i\theta\hat{L}_y), \quad (\text{A16})$$

such that the hybridized modes read

$$\hat{\psi}_s = \hat{R}_y\left(\frac{\pi}{2}\right)\hat{\alpha}\hat{R}_y^\dagger\left(\frac{\pi}{2}\right), \quad \hat{\psi}_a = \hat{R}_y\left(\frac{\pi}{2}\right)\hat{\beta}\hat{R}_y^\dagger\left(\frac{\pi}{2}\right), \quad (\text{A17})$$

which have bosonic commutation relations $[\hat{\psi}_{s/a}, \hat{\psi}_{s/a}^\dagger] = 1$ and $[\hat{\psi}_s, \hat{\psi}_a] = 0$. The relations in Eq. (A17) can be proven straightforwardly with the Baker-Campbell-Hausdorff relation for matrix exponential and mathematical induction. The proof is performed in detail in Appendix E. The rotation operator $\hat{R}_y(\theta)$ [Eq. (A16)] will be convenient when expressing the eigenmodes of $\hat{\mathcal{H}}_{\text{AFM}}$ [Eq. (A8)] and especially important when addressing state control via a qubit in Appendix C.

Now using the hybridized modes $\hat{\psi}_s$ and $\hat{\psi}_a$ [Eq. (A10)], we can transform the full Hamiltonian $\hat{\mathcal{H}}_{\text{AFM}}$ [Eq. (A8)] and obtain the following expression:

$$\begin{aligned}\hat{\mathcal{H}}_{\text{AFM}} = & \omega_s \hat{\psi}_s^\dagger \hat{\psi}_s + \omega_a \hat{\psi}_a^\dagger \hat{\psi}_a + D_s(\hat{\psi}_s^2 + \hat{\psi}_s^{\dagger 2} + \hat{\psi}_a^2 + \hat{\psi}_a^{\dagger 2}) \\ & + (\omega - A).\end{aligned}\quad (\text{A18})$$

In the current form of $\hat{\mathcal{H}}_{\text{AFM}}$ [Eq. (A18)], the hybridized modes $\hat{\psi}_{s/a}$ are decoupled and we can diagonalize their respective contribution to the Hamiltonian separately. We can see that because of the squared terms $\propto D_s$, the Hamiltonian

describes two noninteracting one-mode squeezed harmonic oscillators. Therefore the final step is to perform a one-mode squeezing transformation for both modes, which results in the following diagonalized version of the Hamiltonian:

$$\hat{\mathcal{H}}_{\text{AFM}} = \omega_+ \hat{\psi}_+^\dagger \hat{\psi}_+ + \omega_- \hat{\psi}_-^\dagger \hat{\psi}_- + \frac{\omega_+ + \omega_- - 2A}{2}, \quad (\text{A19})$$

with the one-mode squeezed hybridized modes

$$\begin{aligned} \hat{\psi}_+ &= \cosh(r_+) \hat{\psi}_s + \sinh(r_+) \hat{\psi}_s^\dagger, \\ \hat{\psi}_- &= \cosh(r_-) \hat{\psi}_a + \sinh(r_-) \hat{\psi}_a^\dagger, \end{aligned} \quad (\text{A20})$$

the one mode-squeezing factors

$$\tanh(2r_+) = \frac{2|D_s|}{\omega - D_r}, \quad \tanh(2r_-) = \frac{2|D_s|}{\omega + D_r}, \quad (\text{A21})$$

and the eigenenergies

$$\omega_+ = \sqrt{\omega^2 - 4CD - 4D^2}, \quad \omega_- = \sqrt{\omega^2 + 4CD - 4D^2}. \quad (\text{A22})$$

Here, we want to mention that the one-mode squeeze transformation [Eq. (A20)] can be conveniently expressed via the one-mode squeeze operators

$$\hat{S}_\pm(r_\pm) = \exp\left(\frac{r_\pm}{2}[(\hat{\psi}_{s/a})^2 - (\hat{\psi}_{s/a}^\dagger)^2]\right), \quad (\text{A23})$$

such that the eigenmodes read $\hat{\psi}_+ = \hat{S}_+(r_+) \hat{\psi}_s \hat{S}_+^\dagger(r_+)$ and $\hat{\psi}_- = \hat{S}_-(r_-) \hat{\psi}_a \hat{S}_-^\dagger(r_-)$ [85]. With the relations from Eq. (A17), the eigenmodes can be written as

$$\hat{\psi}_+ = \hat{S}_+(r_+) \hat{R}_y\left(\frac{\pi}{2}\right) \hat{\alpha} \hat{R}_y^\dagger\left(\frac{\pi}{2}\right) \hat{S}_+^\dagger(r_+), \quad (\text{A24})$$

$$\hat{\psi}_- = \hat{S}_-(r_-) \hat{R}_y\left(\frac{\pi}{2}\right) \hat{\beta} \hat{R}_y^\dagger\left(\frac{\pi}{2}\right) \hat{S}_-^\dagger(r_-). \quad (\text{A25})$$

Finally, a general eigenstate of the Hamiltonian $\hat{\mathcal{H}}_{\text{AFM}}$ [Eq. (A8)] with m (n) excitations in the $\hat{\psi}_+$ ($\hat{\psi}_-$) mode can be expressed as

$$|m_+, n_-\rangle = \hat{S}_+(r_+) \hat{S}_-(r_-) \hat{R}_y\left(\frac{\pi}{2}\right) |m_\alpha, n_\beta\rangle, \quad (\text{A26})$$

where $|m_\alpha, n_\beta\rangle$ denotes the eigenstates of $\omega(\hat{\alpha}^\dagger \hat{\alpha} + \hat{\beta}^\dagger \hat{\beta})$ with m (n) denoting the number spin-up (down) magnonic excitations. The relation in Eq. (A26) follows from first considering the vacuum $|0_+, 0_-\rangle$ which has to fulfill $\hat{\psi}_\pm |0_+, 0_-\rangle = 0$. This can be shown straightforwardly

$$\begin{aligned} \hat{\psi}_+ |0_+, 0_-\rangle &= \hat{S}_+(r_+) \hat{R}_y\left(\frac{\pi}{2}\right) \hat{\alpha} \hat{R}_y^\dagger\left(\frac{\pi}{2}\right) \hat{S}_+^\dagger(r_+) \hat{S}_+(r_+) \\ &\quad \times \hat{S}_-(r_-) \hat{R}_y\left(\frac{\pi}{2}\right) |0_\alpha, 0_\beta\rangle \end{aligned} \quad (\text{A27})$$

$$= \hat{S}_+(r_+) \hat{R}_y\left(\frac{\pi}{2}\right) \hat{\alpha} \hat{R}_y^\dagger\left(\frac{\pi}{2}\right) \hat{S}_-(r_-) \hat{R}_y\left(\frac{\pi}{2}\right) |0_\alpha, 0_\beta\rangle \quad (\text{A28})$$

$$= \hat{S}_+(r_+) \hat{S}_-(r_-) \hat{R}_y\left(\frac{\pi}{2}\right) \hat{\alpha} \hat{R}_y^\dagger\left(\frac{\pi}{2}\right) \hat{R}_y\left(\frac{\pi}{2}\right) |0_\alpha, 0_\beta\rangle \quad (\text{A29})$$

$$= \hat{S}_+(r_+) \hat{S}_-(r_-) \hat{R}_y\left(\frac{\pi}{2}\right) \hat{\alpha} |0_\alpha, 0_\beta\rangle \quad (\text{A30})$$

$$= 0, \quad (\text{A31})$$

where we used the property of unitary operators $\hat{S}_+^\dagger(r_+) \hat{S}_+(r_+) = 1$ and $\hat{R}_y^\dagger(\frac{\pi}{2}) \hat{R}_y(\frac{\pi}{2}) = 1$, the commutator $[\hat{R}_y(\frac{\pi}{2}) \hat{\alpha} \hat{R}_y^\dagger(\frac{\pi}{2}), \hat{S}_-(r_-)] = [\hat{\psi}_s, \hat{S}_-(r_-)] = 0$, where we used the relations from Eqs. (A17) and (A23) and $\hat{\alpha} |0_\alpha, 0_\beta\rangle = 0$. From this then follows that

$$|m_+, n_-\rangle = \frac{1}{\sqrt{m!n!}} \hat{\psi}_+^m \hat{\psi}_-^n |0_+, 0_-\rangle \quad (\text{A32})$$

$$\begin{aligned} &= \frac{1}{\sqrt{m!n!}} \hat{S}_+(r_+) \hat{R}_y\left(\frac{\pi}{2}\right) \hat{\alpha}^m \hat{R}_y^\dagger\left(\frac{\pi}{2}\right) \hat{S}_+^\dagger(r_+) \\ &\quad \times \hat{S}_-(r_-) \hat{R}_y\left(\frac{\pi}{2}\right) \hat{\beta}^n \hat{R}_y^\dagger\left(\frac{\pi}{2}\right) \hat{S}_-^\dagger(r_-) \hat{S}_+(r_+) \hat{S}_-(r_-) \\ &\quad \times \hat{R}_y\left(\frac{\pi}{2}\right) |0_\alpha, 0_\beta\rangle \end{aligned} \quad (\text{A33})$$

$$= \frac{1}{\sqrt{m!n!}} \hat{S}_+(r_+) \hat{S}_-(r_-) \hat{R}_y\left(\frac{\pi}{2}\right) \hat{\alpha}^m \hat{\beta}^n |0_\alpha, 0_\beta\rangle \quad (\text{A34})$$

$$= \hat{S}_+(r_+) \hat{S}_-(r_-) \hat{R}_y\left(\frac{\pi}{2}\right) |m_\alpha, n_\beta\rangle, \quad (\text{A35})$$

which shows the relation in Eq. (A26). Note that we also used the commutators $[\hat{R}_y(\frac{\pi}{2}) \hat{\beta} \hat{R}_y^\dagger(\frac{\pi}{2}), \hat{S}_+(r_+)] = [\hat{\psi}_a, \hat{S}_+(r_+)] = 0$ and $[\hat{S}_+(r_+), \hat{S}_-(r_-)] = 0$.

APPENDIX B: PSEUDOSPIN SQUEEZING

In Appendix A 2, we introduce the concept of pseudospin \hat{L} . The pseudospin components fulfill commutation relations $[\hat{L}_i, \hat{L}_j] = i\epsilon_{ijk} \hat{L}_k$ with the Levi-Civita symbol ϵ_{ijk} . Because of that, pseudospin components obey Heisenberg uncertainty relation $\langle \Delta \hat{L}_y^2 \rangle \langle \Delta \hat{L}_x^2 \rangle \geq |\langle \hat{L}_z \rangle|^2 / 4$. In this Appendix, we demonstrate that pseudospin component \hat{L}_y is squeezed according to Heisenberg uncertainty in an eigenstate $|m_+, n_-\rangle$ [Eq. (A26)].

Pseudospin squeezing in a general excited state

In this subsection, we evaluate the expectation values and variances of pseudospin components \hat{L}_i for $i = x, y, z$ for a general eigenstate $|m_+, n_-\rangle$ [Eq. (A26)] with m (n) excitation in eigenmode $\hat{\psi}_+$ ($\hat{\psi}_-$) [Eq. (A20)]. We denote the expectation values by $\langle \hat{L}_i \rangle_{mn} = \langle m_+, n_- | \hat{L}_i | m_+, n_- \rangle$ and the variances $\langle \Delta \hat{L}_i^2 \rangle_{mn} = \langle m_+, n_- | \hat{L}_i^2 | m_+, n_- \rangle - \langle \hat{L}_i \rangle_{mn}^2$. We find the following expectation values:

$$\begin{aligned} \langle \hat{L}_x \rangle_{mn} &= \frac{m(\cosh^2 r_+ + \sinh^2 r_+) + \sinh^2 r_+}{2} \\ &\quad - \frac{n(\cosh^2 r_- + \sinh^2 r_-) + \sinh^2 r_-}{2}, \end{aligned} \quad (\text{B1})$$

and $\langle \hat{L}_y \rangle_{mn} = \langle \hat{L}_z \rangle_{mn} = 0$. The corresponding variances of interest read

$$\begin{aligned} \langle \Delta \hat{L}_y^2 \rangle_{mn} &= \frac{2mn + m + n}{4} (\cosh r_+ \cosh r_- - \sinh r_+ \sinh r_-)^2 \\ &\quad + \frac{2mn + m + n + 1}{4} (\sinh r_+ \cosh r_- \\ &\quad - \sinh r_- \cosh r_+)^2, \end{aligned} \quad (\text{B2})$$

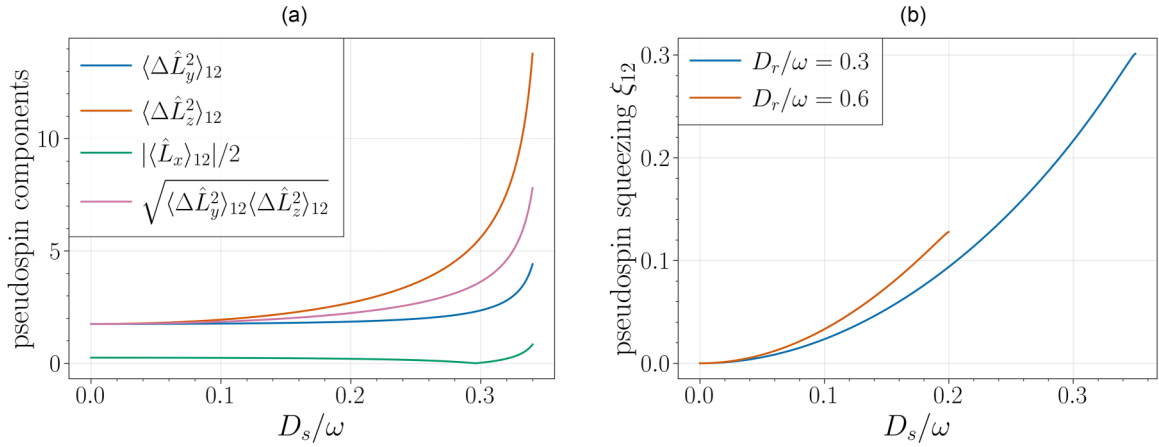


FIG. 6. Plot of (a) pseudospin components and variances $|\langle \hat{L}_x \rangle_{12}|$, $\langle \Delta \hat{L}_y^2 \rangle_{12}$, and $\langle \Delta \hat{L}_z^2 \rangle_{12}$ in the eigenstate $|1, 2\rangle$ for fixed $D_r/\omega = 0.3$ and (b) pseudospin squeezing ξ_{12} as a function of D_s .

$$\begin{aligned} \langle \Delta \hat{L}_z^2 \rangle_{mn} &= \frac{2mn + m + n}{4} (\cosh r_+ \cosh r_- + \sinh r_+ \sinh r_-)^2 \\ &+ \frac{2mn + m + n + 1}{4} (\sinh r_+ \cosh r_- \\ &+ \sinh r_- \cosh r_+)^2. \end{aligned} \quad (\text{B3})$$

Neglecting the intrasublattice coupling D_s , we find

$$\langle \hat{L}_x \rangle_{mn} = \frac{m - n}{2}, \quad (\text{B4})$$

$$\langle \Delta \hat{L}_y^2 \rangle_{mn} = \frac{2mn + m + n}{4}, \quad (\text{B5})$$

$$\langle \Delta \hat{L}_z^2 \rangle_{mn} = \frac{2mn + m + n}{4}, \quad (\text{B6})$$

such that $\langle \Delta \hat{L}_y^2 \rangle_{mn} = \langle \Delta \hat{L}_z^2 \rangle_{mn}$. From this, we can deduce that if $D_s = 0$, there is no squeezing present since the variances of \hat{L}_y and \hat{L}_z are the same.

As in the main text, let us analyze a simpler case with $m \neq 0$, $n = 0$ and $D_s \neq 0$. We find that the expectation value of \hat{L}_x and the variances of \hat{L}_y and \hat{L}_z [Eqs. (B1)–(B3)] reduce to the following expressions:

$$\langle \hat{L}_x \rangle_{m0} = \frac{m + \frac{1}{2}}{2} \cosh 2r_+ - \frac{\cosh 2r_-}{4}, \quad (\text{B7})$$

$$\langle \Delta \hat{L}_y^2 \rangle_{m0} = \frac{m + \frac{1}{2}}{4} \cosh (2r_+ - 2r_-) - \frac{1}{8}, \quad (\text{B8})$$

$$\langle \Delta \hat{L}_z^2 \rangle_{m0} = \frac{m + \frac{1}{2}}{4} \cosh (2r_+ + 2r_-) - \frac{1}{8}. \quad (\text{B9})$$

After some algebra, we find the following uncertainty relation:

$$\langle \Delta \hat{L}_y^2 \rangle_{m0} \langle \Delta \hat{L}_z^2 \rangle_{m0} = \frac{1}{4} |\langle \hat{L}_x \rangle_{m0}|^2 + \frac{m^2 + m}{8} (\cosh 4r_- - 1), \quad (\text{B10})$$

so that the state we consider here is not minimum uncertainty. We check if $\langle \Delta \hat{L}_y^2 \rangle_{m0} < \frac{1}{2} |\langle \hat{L}_x \rangle_{m0}|^2$ is fulfilled and find that this condition is equivalent to

$$(2m + 1)(\cosh 2r_+ - \cosh(2r_+ - 2r_-)) > \cosh 2r_- - 1. \quad (\text{B11})$$

This is fulfilled if $r_- > 0$ and $r_+ > r_-$. This means that L_y is squeezed with respect to L_x and that $\langle \Delta \hat{L}_y^2 \rangle < \langle \Delta \hat{L}_z^2 \rangle$. We can quantify squeezing by the ellipticity of Heisenberg's uncertainty relation [Eq. (B10)] [2], defining

$$\langle \Delta \hat{L}_y^2 \rangle_{mn} = e^{-2\xi_{mn}} \sqrt{\langle \Delta \hat{L}_y^2 \rangle_{mn} \langle \Delta \hat{L}_z^2 \rangle_{mn}}, \quad (\text{B12})$$

$$\langle \Delta \hat{L}_z^2 \rangle_{mn} = e^{2\xi_{mn}} \sqrt{\langle \Delta \hat{L}_y^2 \rangle_{mn} \langle \Delta \hat{L}_z^2 \rangle_{mn}}, \quad (\text{B13})$$

with pseudospin squeezing factor ξ_{mn} . Squeezing factor ξ_{mn} is explicitly given by

$$\xi_{mn} = -\frac{1}{4} \ln \frac{\langle \Delta \hat{L}_y^2 \rangle_{mn}}{\langle \Delta \hat{L}_z^2 \rangle_{mn}}. \quad (\text{B14})$$

In the main text, we mention that pseudospin squeezing ξ_{m0} for $m \neq 0$ and $n = 0$ has a finite value $\xi_{\text{inst}} \approx r_-$ at the instability $2|D_s| = 1 - D_r$. This can be shown, by rewriting ξ_{m0} in the following way:

$$\xi_{m0} = -\frac{1}{4} \ln \left(\frac{(m + \frac{1}{2})(e^{-2r_-} + e^{-4r_+ + 2r_-}) - e^{-2r_+}}{(m + \frac{1}{2})(e^{2r_-} + e^{-4r_+ - 2r_-}) - e^{-2r_+}} \right). \quad (\text{B15})$$

At the instability, the $\hat{\psi}_+$ mode becomes unstable as quadrature squeezing diverges $r_+ \rightarrow \infty$. We therefore use the approximation $\exp(-r_+) \approx 0$, such that pseudospin squeezing at the instability becomes

$$\xi_{\text{inst}} \approx -\frac{1}{4} \ln \left(\frac{e^{-2r_-}}{e^{2r_-}} \right), \quad (\text{B16})$$

which is equivalent to $\xi_{\text{inst}} \approx r_-$.

Having discussed squeezing for a state $|m_+, 0_- \rangle$, we now want to evaluate Heisenberg's uncertainty relation graphically for states with $m \neq 0$ and $n \neq 0$ in Fig. 6(a). One can see for $m = 1$ and $n = 2$, on the one hand, $|\langle \hat{L}_x \rangle_{12}|/2 < \langle \Delta \hat{L}_y^2 \rangle_{12}$, and therefore fluctuations are larger than the ground-state fluctuations. On the other hand, the variances fulfill $\sqrt{\langle \Delta \hat{L}_y^2 \rangle_{12}} < \sqrt{\langle \Delta \hat{L}_z^2 \rangle_{12}}$ and hence follows squeezing according to the definition via ellipticity.

APPENDIX C: COUPLING TO SPIN QUBIT

In this Appendix, we analyze the interaction between an antiferromagnet with strong intrasublattice coupling as described by $\hat{\mathcal{H}}_{\text{AFM}}$ [Eq. (A8)] and a spin qubit in the dispersive regime. In Appendix C 1, we derive the direct dispersive coupling from a spin Hamiltonian. In Appendix C 2, we diagonalize the resulting Hamiltonian describing the AFM, qubit and direct dispersive coupling and discuss state control via the qubit. Finally, in Appendix C 3 we discuss if pseudospin squeezing can be resolved via qubit spectroscopy. Here we focus on the signatures of pseudospin squeezing in two coupling regimes.

1. Dispersive coupling

In this subsection, we derive the direct dispersive coupling between the AFM and the spin qubit. The Hamiltonian describing the spin qubit is given by $\hat{\mathcal{H}}_q = \omega_q \hat{\sigma}_z / 2$, where ω_q denotes the level splitting of the qubit and $\hat{\sigma}_z$ the third Pauli matrix. We assume that the AFM and qubit interact via exchange interaction between the spin qubit and the spins belonging to the AFM interfacing with the qubit [62,66,84]. This interaction can be described by the following Hamiltonian:

$$\hat{\mathcal{H}}_{\text{int}} = J_{\text{int},A} \sum_{l \in A} \hat{\mathbf{S}}_l \cdot \hat{\mathbf{s}}_l + J_{\text{int},B} \sum_{m \in B} \hat{\mathbf{S}}_m \cdot \hat{\mathbf{s}}_m, \quad (\text{C1})$$

where l and m label the interfacial site belonging to sublattices A and B , $J_{\text{int},A(B)}$ is the interfacial coupling strength [86–89] with lattice site belonging to sublattice $A(B)$, $\hat{\mathbf{S}}$ denotes the spin operator and $\hat{\mathbf{s}}$ spin of the electronic states comprising the qubit. As argued in Refs. [84,66,67], terms $\propto \hat{S}_i^x \hat{s}_i^x$ and $\propto \hat{S}_i^y \hat{s}_i^y$ result in a coherent interaction, leading to a hybridization between magnons and the qubit. Here, we want to suppress coherent exchange by choosing a large detuning between the magnon resonance frequency ω and the qubit level splitting ω_q and hence focus on the terms $\propto \hat{S}_i^z \hat{s}_i^z$. Using Holstein-Primakoff transformations [Eq. (A2)], we find that the terms $\propto \hat{S}_i^z \hat{s}_i^z$ in the interaction Hamiltonian $\hat{\mathcal{H}}_{\text{int}}$ [Eq. (C1)] have one constant term renormalizing the qubit level splitting [84] and a coupling term resulting in dispersive interaction [66]

$$\hat{\mathcal{H}}_{\text{dis}} = |\phi|^2 \left(\frac{J_{\text{int},A} N_{\text{int},A}}{2N} \hat{a}^\dagger \hat{a} - \frac{J_{\text{int},B} N_{\text{int},B}}{2N} \hat{b}^\dagger \hat{b} \right) \hat{\sigma}_z, \quad (\text{C2})$$

where $|\phi_l|$ denotes the qubit wave function at lattice site l , which here is assumed to be homogeneous [66,84], and $N_{\text{int},A(B)}$ the number of interfacial lattice sites belonging to sublattice $A(B)$.

Defining the direct dispersive coupling strengths

$$\chi_a = \frac{J_{\text{int},A} |\phi|^2}{2N} N_{\text{int},A}, \quad \chi_b = \frac{J_{\text{int},B} |\phi|^2}{2N} N_{\text{int},B}, \quad (\text{C3})$$

we can deduce that the coupling between the AFM and qubit depends on the size of the magnet and the structure of the interface. Assuming a compensated magnet with a compensated interface, such that $\chi_a = \chi_b \equiv \chi$, and using the Bogoliubov transformation [Eq. (A6)], the direct dispersive interaction Hamiltonian $\hat{\mathcal{H}}_{\text{dis}}$ [Eq. (C2)] acquires the form used in the main text $\hat{\mathcal{H}}_{\text{dis}} = 2\chi \hat{L}_z \hat{\sigma}_z$.

2. Eigenmodes of the coupled AFM and qubit system

In this subsection, we diagonalize the Hamiltonian describing an AFM with strong intrasublattice interaction coupled to a spin qubit via direct dispersive coupling. The full Hamiltonian is given by a sum of the AFM Hamiltonian $\hat{\mathcal{H}}_{\text{AFM}}$ [Eq. (A8)], $\hat{\mathcal{H}}_q = \omega_q \hat{\sigma}_z / 2$ and the direct dispersive interaction $\hat{\mathcal{H}}_{\text{dis}}$ [Eq. (C2)]. Here, we assume $\chi_a = \chi_b \equiv \chi$ [Eq. (C3)], such that the full Hamiltonian in spin-up and spin-down magnon basis reads

$$\hat{\mathcal{H}}_0 = \hat{\mathcal{H}}_{\text{AFM}} + \frac{\omega_q}{2} \hat{\sigma}_z + \chi (\hat{\alpha}^\dagger \hat{\alpha} - \hat{\beta}^\dagger \hat{\beta}) \hat{\sigma}_z, \quad (\text{C4})$$

with $\hat{\mathcal{H}}_{\text{AFM}}$ from Eq. (A8). We start the analysis by projecting the full Hamiltonian $\hat{\mathcal{H}}_0$ [Eq. (C4)] onto the qubit eigenstates, which are given by the ground state $|g\rangle$ and excited state $|e\rangle$. We define the reduced Hamiltonians by

$$\hat{\mathcal{H}}_g = \langle g | \hat{\mathcal{H}}_0 | g \rangle, \quad \hat{\mathcal{H}}_e = \langle e | \hat{\mathcal{H}}_0 | e \rangle. \quad (\text{C5})$$

In the following, we treat $\hat{\mathcal{H}}_g$ [Eq. (C5)] in detail and afterwards transfer our results to $\hat{\mathcal{H}}_e$ [Eq. (C5)] via the substitutions $-\omega_q \rightarrow +\omega_q$ and $-\chi \rightarrow +\chi$. We diagonalize $\hat{\mathcal{H}}_g$ using the pseudospin framework with pseudospin operators \hat{L}_i , $i = 0, 1, 2, 3$ [Eq. (A13)]. Following Ref. [43], we separate $\hat{\mathcal{H}}_g$ [Eq. (C5)] in a base Hamiltonian and perturbation Hamiltonian, such that $\hat{\mathcal{H}}_g = \hat{\mathcal{H}}_{\text{base}}^g + \hat{\mathcal{H}}_{\text{pert}}^g$ with

$$\hat{\mathcal{H}}_{\text{base}}^g = \omega (\hat{\alpha}^\dagger \hat{\alpha} + \hat{\beta}^\dagger \hat{\beta}) + \frac{2\omega - 2A - \omega_q}{2}, \quad (\text{C6})$$

$$\hat{\mathcal{H}}_{\text{pert,hyb}}^g = -\chi (\hat{\alpha}^\dagger \hat{\alpha} - \hat{\beta}^\dagger \hat{\beta}) - D_r (\hat{\alpha} \hat{\beta}^\dagger + \hat{\alpha}^\dagger \hat{\beta}), \quad (\text{C7})$$

$$\hat{\mathcal{H}}_{\text{pert,quad}}^g = D_s (\hat{\alpha}^2 + \hat{\alpha}^{\dagger 2} + \hat{\beta}^2 + \hat{\beta}^{\dagger 2}). \quad (\text{C8})$$

Here, we divided the perturbation into two parts, the hybridization Hamiltonian $\hat{\mathcal{H}}_{\text{pert,hyb}}^g$ [Eq. (C7)] and quadratic terms $\hat{\mathcal{H}}_{\text{pert,quad}}^g$ [Eq. (C8)]. We begin by treating $\hat{\mathcal{H}}_{\text{base}}^g + \hat{\mathcal{H}}_{\text{pert,hyb}}^g$ in the pseudospin framework [43], reformulating $\hat{\mathcal{H}}_{\text{base}}^g + \hat{\mathcal{H}}_{\text{pert,hyb}}^g$ with pseudospin operators \hat{L}_i , $i = 0, 1, 2, 3$, and obtain

$$\hat{\mathcal{H}}_{\text{base}}^g + \hat{\mathcal{H}}_{\text{pert,hyb}}^g = 2\omega \hat{L}_0 - \omega^g \cdot \hat{\mathbf{L}} + \frac{2\omega - 2A - \omega_q}{2}, \quad (\text{C9})$$

with pseudofield

$$\omega^g = 2D_r \hat{e}_x + 2\chi \hat{e}_z. \quad (\text{C10})$$

Here, we can already notice that pseudofield ω^g [Eq. (C10)] acquires a z component from the interaction with the spin qubit in comparison with ω^0 (with $\chi = 0$). As discussed in Appendix A 2, the eigenmodes of a Hamiltonian of the form of $\hat{\mathcal{H}}_{\text{base}}^g + \hat{\mathcal{H}}_{\text{pert,hyb}}^g$ [Eq. (C9)] can be conveniently characterized by the pseudofield ω^g [Eq. (C10)] and a rotation operation [Eq. (A17)]. The eigenmodes of $\hat{\mathcal{H}}_{\text{base}}^g + \hat{\mathcal{H}}_{\text{pert,hyb}}^g$ [Eq. (C9)] can therefore be expressed as

$$\hat{\psi}_1^g = \hat{R}_y(\theta_g) \hat{\alpha} \hat{R}_y^\dagger(\theta_g), \quad \hat{\psi}_2^g = \hat{R}_y(\theta_g) \hat{\beta} \hat{R}_y^\dagger(\theta_g), \quad (\text{C11})$$

with rotation operator $\hat{R}_y(\theta)$ [Eq. (A16)] and rotation angle $\sin \theta_g = 1/\sqrt{1 + \chi^2/D_r^2}$. It will be convenient to define a small angle $\tilde{\theta}$ such that $\theta_g = \frac{\pi}{2} - \tilde{\theta}$, which explicitly reads

$$\sin \tilde{\theta} = |\chi|/\sqrt{\chi^2 + D_r^2}. \quad (\text{C12})$$

Transforming the full Hamiltonian $\hat{\mathcal{H}}_g$ [Eq. (C5)] into the basis of $\hat{\psi}_1^g$ and $\hat{\psi}_2^g$ [Eq. (C11)], we obtain the expression

$$\hat{\mathcal{H}}_g = \omega_1^g \hat{\psi}_1^{g\dagger} \hat{\psi}_1^g + \omega_2^g \hat{\psi}_2^{g\dagger} \hat{\psi}_2^g + D_s (\hat{\psi}_1^{g2} + \hat{\psi}_1^{g\dagger 2} + \hat{\psi}_2^{g2} + \hat{\psi}_2^{g\dagger 2}) + \frac{2\omega - 2A - \omega_q}{2}, \quad (\text{C13})$$

with frequencies

$$\omega_1^g = \omega - \sqrt{\chi^2 + D_r^2}, \quad \omega_2^g = \omega + \sqrt{\chi^2 + D_r^2}. \quad (\text{C14})$$

Now $\hat{\psi}_1^g$ and $\hat{\psi}_2^g$ decouple and we can solve $\hat{\mathcal{H}}_g$ [Eq. (C13)] by applying a one-mode squeezing transformation. We end up with the diagonalized Hamiltonian

$$\hat{\mathcal{H}}_g = \omega_1^{g,\text{sq}} \hat{\psi}_1^{g,\text{sq}\dagger} \hat{\psi}_1^{g,\text{sq}} + \omega_2^{g,\text{sq}} \hat{\psi}_2^{g,\text{sq}\dagger} \hat{\psi}_2^{g,\text{sq}} + \frac{\omega_1^{g,\text{sq}} + \omega_2^{g,\text{sq}} - 2A - \omega_q}{2}, \quad (\text{C15})$$

where the eigenmodes $\hat{\psi}_{1/2}^{g,\text{sq}}$ can be expressed as

$$\hat{\psi}_1^{g,\text{sq}} = \hat{S}_{g,1}^{\text{oms}}(r_1^g) \hat{\psi}_1^g \hat{S}_{g,1}^{\text{oms}}(r_1^g)^\dagger, \quad \hat{\psi}_2^{g,\text{sq}} = \hat{S}_{g,2}^{\text{oms}}(r_2^g) \hat{\psi}_2^g \hat{S}_{g,2}^{\text{oms}}(r_2^g)^\dagger, \quad (\text{C16})$$

with squeeze operators

$$\hat{S}_{g,1/2}^{\text{oms}}(r_{1/2}^g) = \exp\left(\frac{\tilde{r}}{2}[(\hat{\psi}_{1/2}^g)^2 - (\hat{\psi}_{1/2}^{g\dagger})^2]\right), \quad (\text{C17})$$

and one mode-squeezing factors

$$\tanh(2r_1^g) = \frac{2|D_s|}{\omega - \sqrt{\chi^2 + D_r^2}}, \quad \tanh(2r_2^g) = \frac{2|D_s|}{\omega + \sqrt{\chi^2 + D_r^2}}. \quad (\text{C18})$$

The eigenenergies in $\hat{\mathcal{H}}_g$ [Eq. (C15)] read

$$\omega_1^{g,\text{sq}} = \sqrt{\omega^2 - 2\omega\sqrt{\chi^2 + D_r^2} + \chi^2 - 4D^2}, \quad (\text{C19})$$

$$\omega_2^{g,\text{sq}} = \sqrt{\omega^2 + 2\omega\sqrt{\chi^2 + D_r^2} + \chi^2 - 4D^2}. \quad (\text{C20})$$

Combining Eqs. (C11) and (C16) allows us to write the eigenmodes of $\hat{\mathcal{H}}_g$ [Eq. (C15)] in the following compact form:

$$\hat{\psi}_1^{g,\text{sq}} = \hat{S}_{g,1}^{\text{oms}}(r_1^g) \hat{R}_y\left(\frac{\pi}{2} - \tilde{\theta}\right) \hat{\alpha} \hat{R}_y^\dagger\left(\frac{\pi}{2} - \tilde{\theta}\right) \hat{S}_{g,1}^{\text{oms}}(r_1^g)^\dagger, \quad (\text{C21})$$

$$\hat{\psi}_2^{g,\text{sq}} = \hat{S}_{g,2}^{\text{oms}}(r_2^g) \hat{R}_y\left(\frac{\pi}{2} - \tilde{\theta}\right) \hat{\beta} \hat{R}_y^\dagger\left(\frac{\pi}{2} - \tilde{\theta}\right) \hat{S}_{g,2}^{\text{oms}}(r_2^g)^\dagger, \quad (\text{C22})$$

which is an equivalent form as Eqs. (A24) and (A25) from Appendix A 2.

Now we evaluate the diagonalization of the excited state Hamiltonian $\hat{\mathcal{H}}_e$ [Eq. (C5)] that can be obtained from the solution of $\hat{\mathcal{H}}_g$ [Eq. (C15)] via the substitutions $-\omega_q \rightarrow +\omega_q$ and $-\chi \rightarrow +\chi$. Note that we also perform an index substitution $g \rightarrow e$ to indicate entities belonging to the excited state manifold. We find the angle $\theta_e = \pi/2 - \tilde{\theta}$ [Eq. (C12)], the squeeze factors $r_1^e = r_1^g \equiv r_1$ and $r_2^e = r_2^g \equiv r_2$ [Eq. (C18)] and the eigenenergies $\omega_1^{e,\text{sq}} = \omega_1^{g,\text{sq}}$ and $\omega_2^{e,\text{sq}} = \omega_2^{g,\text{sq}}$ [Eqs. (C19) and (C20)]. The diagonalized Hamiltonian $\hat{\mathcal{H}}_e$

[Eq. (C5)] reads

$$\hat{\mathcal{H}}_e = \omega_1^{\text{sq}} \hat{\psi}_1^{e,\text{sq}\dagger} \hat{\psi}_1^{e,\text{sq}} + \omega_2^{\text{sq}} \hat{\psi}_2^{e,\text{sq}\dagger} \hat{\psi}_2^{e,\text{sq}} + \frac{\omega_1^{\text{sq}} + \omega_2^{\text{sq}} - 2A + \omega_q}{2}. \quad (\text{C23})$$

Equivalently to the expressions for $\hat{\psi}_{1/2}^{g,\text{sq}}$ in Eqs. (C21) and (C22), the eigenmodes $\hat{\psi}_{1/2}^{e,\text{sq}}$ can be obtained by applying the following operations:

$$\hat{\psi}_1^{e,\text{sq}} = \hat{S}_{e,1}^{\text{oms}}(r_1) \hat{R}_y\left(\frac{\pi}{2} + \tilde{\theta}\right) \hat{\alpha} \hat{R}_y^\dagger\left(\frac{\pi}{2} + \tilde{\theta}\right) \hat{S}_{e,1}^{\text{oms}}(r_1)^\dagger, \quad (\text{C24})$$

$$\hat{\psi}_2^{e,\text{sq}} = \hat{S}_{e,2}^{\text{oms}}(r_2) \hat{R}_y\left(\frac{\pi}{2} + \tilde{\theta}\right) \hat{\beta} \hat{R}_y^\dagger\left(\frac{\pi}{2} + \tilde{\theta}\right) \hat{S}_{e,2}^{\text{oms}}(r_2)^\dagger, \quad (\text{C25})$$

with the one-mode squeeze operators

$$\hat{S}_{e,1/2}^{\text{oms}}(r_{1/2}) = \exp\left(\frac{r_{1/2}}{2}[(\hat{\psi}_{1/2}^e)^2 - (\hat{\psi}_{1/2}^{e\dagger})^2]\right). \quad (\text{C26})$$

Using a similar technique and proof as for Eq. (A26) in Appendix A 2, we can determine the eigenstates of $\hat{\mathcal{H}}_g$ and $\hat{\mathcal{H}}_e$ [Eqs. (C15) and (C23)]. We find that they can be expressed as

$$|m, n\rangle_g = \hat{S}_{g,1}^{\text{oms}}(r_1) \hat{S}_{g,2}^{\text{oms}}(r_2) \hat{R}_y\left(\frac{\pi}{2} - \tilde{\theta}\right) |m_\alpha, n_\beta\rangle, \quad (\text{C27})$$

$$|m, n\rangle_e = \hat{S}_{e,1}^{\text{oms}}(r_1) \hat{S}_{e,2}^{\text{oms}}(r_2) \hat{R}_y\left(\frac{\pi}{2} + \tilde{\theta}\right) |m_\alpha, n_\beta\rangle, \quad (\text{C28})$$

where $|m, n\rangle_{g/e}$ denotes a Fock state of $\hat{\mathcal{H}}_{g/e}$ [Eqs. (C15) and (C23)] and $|m_\alpha, n_\beta\rangle$ an eigenstate of $\omega(\hat{\alpha}^\dagger \hat{\alpha} + \hat{\beta}^\dagger \hat{\beta})$. We can conclude from this result that the nature of eigenmodes stays the same as in the analysis in Appendix A 2 but the interaction with a qubit modifies the rotation angle of pseudospin as well as the one-mode squeezing of the eigenmodes. The fact that the rotation angle depends on the state of the qubit ($|g\rangle$ or $|e\rangle$) shows that a qubit can be used for state control of pseudospin.

3. Ground-state composition

In this subsection, we discuss if pseudospin squeezing as defined in Appendix B manifests itself via a characteristic signature in qubit spectroscopy [90–92]. For this purpose, we follow the method in Refs. [66,67] and investigate if there is a nonvanishing overlap between the ground state $|0, 0\rangle_g$ [Eq. (C27)] and an excited state $|m, n\rangle_e$ [Eq. (C28)].

If there is a nonvanishing overlap between the ground state and an excited state $\langle m, n | 0, 0 \rangle_g \neq 0$ and the qubit is driven, e.g., by an external microwave drive, at a frequency that matches the energy difference between the states $|0, 0\rangle_g$ and $|m, n\rangle_e$, then the transition $|0, 0\rangle_g \rightarrow |m, n\rangle_e$ occurs with a probability of $|\langle m, n | 0, 0 \rangle_g|^2$. When performing qubit spectroscopy by driving the qubit in a range of frequencies and measuring its population, the excitation probability $|\langle m, n | 0, 0 \rangle_g|^2$ should manifest itself in as a nontrivial peak.

Our goal in the following is to find out if there are excited states $|m, n\rangle_e$ [Eq. (C28)] that have a nonvanishing overlap with the ground state $|0, 0\rangle_g$ [Eq. (C27)], hence demonstrating if pseudospin squeezing has a nontrivial signature in qubit spectroscopy. However, since the operators $\hat{\psi}_1^g$ and $\hat{\psi}_2^g$ don't commute with $\hat{\psi}_1^{e\dagger}$ and $\hat{\psi}_2^{e\dagger}$, the analytical calculation of the overlap is a nontrivial task. We therefore expand the operators in the two limits $\chi/D_r \ll 1$ and $D_r/\chi \ll 1$ and calculate the overlap in these limits.

a. Small χ limit

We begin our analysis with the small χ limit. If $|\chi| \ll |D_r|$, then the angle $\tilde{\theta}$ [Eq. (C12)] becomes

$$\tilde{\theta} \approx \frac{\chi}{|D_r|}, \quad (\text{C29})$$

and correspondingly $\cos \tilde{\theta} \approx \text{sng}(D)$ and $\sin \tilde{\theta} \approx \tilde{\theta}$. Under the same condition $|\chi| \ll |D_r|$, the squeezing factors r_1 and r_2 [Eq. (C18)] simplify to

$$r_1 \approx r_+ + \mathcal{O}(\chi^2), \quad r_2 \approx r_- + \mathcal{O}(\chi^2), \quad (\text{C30})$$

with the squeeze factors r_+ and r_- [Eq. (A21)]. Since $\tilde{\theta}$ is first order in χ and therefore a small parameter, we will express the expansion of operators in terms of $\tilde{\theta}$. The rotation operator $\hat{R}_y(\theta)$ [Eq. (A16)] becomes

$$\hat{R}_y(\pm\tilde{\theta}) \approx \mathbb{I} \pm \frac{\tilde{\theta}}{2} (\hat{\psi}_s \hat{\psi}_a^\dagger - \hat{\psi}_s^\dagger \hat{\psi}_a), \quad (\text{C31})$$

with hybridized modes $\hat{\psi}_{s/a}$ [Eq. (A10)]. We note that the one-mode squeezing operators [Eqs. (C17) and (C26)] are related via the following relations:

$$\hat{S}_{g,1}^{\text{oms}}(r_+) = \hat{R}_y(-2\tilde{\theta}) \hat{S}_{e,1}^{\text{oms}}(r_+) \hat{R}_y(2\tilde{\theta}), \quad (\text{C32})$$

$$\hat{S}_{g,2}^{\text{oms}}(r_-) = \hat{R}_y(-2\tilde{\theta}) \hat{S}_{e,2}^{\text{oms}}(r_-) \hat{R}_y(2\tilde{\theta}), \quad (\text{C33})$$

which we will use to determine the overlaps between the ground state $|0, 0\rangle_g$ and excited states $|m, n\rangle_e$ [Eqs. (C27) and (C28)]. Keeping terms up to first order in χ , we find that the $|0, 0\rangle_g$ [Eq. (C27)] can be expanded in terms of excited $|m, n\rangle_e$ [Eq. (C28)] via the following expression:

$$|0, 0\rangle_g \approx |0, 0\rangle_e + \tilde{\theta} c_1 |1, 1\rangle_e, \quad (\text{C34})$$

with coefficient

$$c_1 = -\frac{\sinh(r_+ - r_-)}{2}. \quad (\text{C35})$$

From Eqs. (C15) and (C23), we deduce that the energy difference between states $|0, 0\rangle_e$ and $|0, 0\rangle_g$ is given by $\omega_{00} = \omega_q$ and the energy difference between $|1, 1\rangle_e$ and $|0, 0\rangle_g$ reads $\omega_{11} = \omega_q + \omega_1^{\text{sq}} + \omega_2^{\text{sq}}$ with $\omega_{1/2}^{\text{sq}}$ from Eqs. (C19) and (C20). When driving the qubit at frequency ω_{11} , the transition into state $|1, 1\rangle_e$ occurs with a probability of $\theta^2 |c_1|^2$. Therefore, qubit spectroscopy would reveal a nontrivial peak around ω_{11} with a peak height proportional to the transition probability $\theta^2 |c_1|^2$. Considering $D_s = 0$, we find that the overlap vanishes $c_1 = 0$ which reproduces the result for an AFM with $D_s = 0$ with a compensated interface [67].

b. Small D_r limit

The small $D_r \rightarrow 0$ limit has to be treated separately, since it is dictated by the condition $|D_r| \ll |\chi|$. The angle $\tilde{\theta}$ [Eq. (C12)] in the small D_r limit becomes

$$\tilde{\theta} \approx \frac{\pi}{2} - \frac{|D_r|}{\chi}, \quad (\text{C36})$$

and correspondingly $\cos \tilde{\theta} \approx |D_r|/\chi$ and $\sin \tilde{\theta} \approx \text{sgn}(D_r)$. The squeeze factors r_1 and r_2 [Eq. (C18)] in the small D_r limit

read

$$\begin{aligned} \tanh(2r_1) &\approx \frac{2|D_s|}{\omega - |\chi|} + \mathcal{O}(D_r^2), \\ \tanh(2r_2) &\approx \frac{2|D_s|}{\omega + |\chi|} + \mathcal{O}(D_r^2). \end{aligned} \quad (\text{C37})$$

Here, we consider the zeroth order in D_r and therefore take the angle $\tilde{\theta}$ to be $\tilde{\theta} = \pi/2$. We can express the ground state $|0, 0\rangle_g$ [Eq. (C27)] and excited state $|0, 0\rangle_e$ [Eq. (C27)] as

$$\begin{aligned} |0, 0\rangle_g &= \hat{S}_\alpha(r_1) \hat{S}_\beta(r_2) |0_\alpha, 0_\alpha\rangle, \\ |0, 0\rangle_e &= \hat{S}_\beta(r_1) \hat{S}_\alpha(r_2) |0_\alpha, 0_\alpha\rangle, \end{aligned} \quad (\text{C38})$$

where we used that $\hat{\psi}_1^g = \hat{\alpha}$, $\hat{\psi}_2^g = \hat{\beta}$, $\hat{\psi}_1^e = \hat{\beta}$, and $\hat{\psi}_2^e = \hat{\alpha}$ if $\tilde{\theta} = \pi/2$. Note that we defined the squeeze operators $\hat{S}_\alpha(r) = \exp(r[\hat{\alpha}^2 - \hat{\alpha}^{\dagger 2}]/2)$ and $\hat{S}_\beta(r) = \exp(r[\hat{\beta}^2 - \hat{\beta}^{\dagger 2}]/2)$. Since $|0, 0\rangle_g$ and $|0, 0\rangle_e$ [Eq. (C38)] can be expressed in a common basis, we can connect the two states via the following relation:

$$|0, 0\rangle_g = \hat{S}_\alpha(r_1 - r_2) \hat{S}_\beta(r_2 - r_1) |0, 0\rangle_e. \quad (\text{C39})$$

The expansion of the ground state $|0, 0\rangle_g$ in terms of excited states $|m, n\rangle_e$ then reads

$$|0, 0\rangle_g \approx c_{mn} |2m, 2n\rangle_e, \quad (\text{C40})$$

with

$$c_{mn} = \frac{(-1)^n}{\cosh(r_{\text{eff}})} \tanh[m + n](r_{\text{eff}}) \frac{\sqrt{(2m)!(2n)!}}{2^m m! 2^n n!}, \quad (\text{C41})$$

and $r_{\text{eff}} = r_1 - r_2$. This result is consistent with Ref. [66] and corresponds to the signature of two decoupled ferromagnets with anisotropies.

APPENDIX D: HEMATITE (α -Fe₂O₃) AND ADJUSTMENTS IN FORMALISM

In this Appendix, we discuss the antiferromagnet hematite (α -Fe₂O₃) above the Morin temperature $T_M \approx 250$ K [93], when it is in the canted phase. We first derive the Hamiltonian from a spin model and see that there is a slight modification in comparison with the Hamiltonian discussed in Appendix A.1. We then discuss how this modification can be incorporated into the theory developed in the main text.

We start with a spin model on a bipartite lattice, consisting of sublattice A and B , and consider spin exchange interaction, easy-plane anisotropy and Dzyaloshinskii–Moriya interaction (DMI) and an applied magnetic field along the y axis [94–97],

$$\begin{aligned} \mathcal{H}_{\text{hem}} &= J \sum_{\langle i, j \rangle} \hat{\mathbf{S}}_i \cdot \hat{\mathbf{S}}_j + K \sum_{i \in A, j \in B} [(\hat{S}_i^x)^2 + (\hat{S}_j^x)^2] \\ &\quad + \mathcal{D} \sum_{\langle i, j \rangle} \hat{\mathbf{x}} \cdot [\hat{\mathbf{S}}_i \times \hat{\mathbf{S}}_j] \\ &\quad - \gamma \mu_0 H_0 \sum_{i \in A, j \in B} (\hat{S}_i^y + \hat{S}_j^y), \end{aligned} \quad (\text{D1})$$

where J denotes the exchange integral, K the anisotropy coefficient, \mathcal{D} the DMI strength, and H_0 the magnitude of the applied magnetic field. Following Refs. [98, 44], we use the

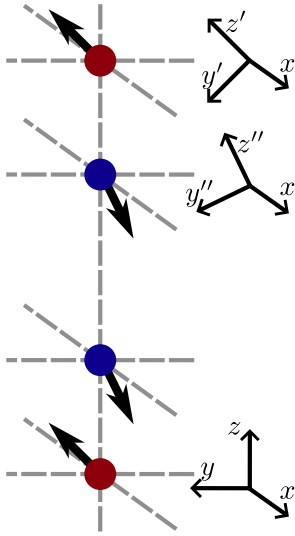


FIG. 7. Canted ground state of hematite above Morin temperature T_M . The spins of the down spin sublattice (depicted in blue) point along the $-z''$ direction, whereas the spin of the up-spin sublattice (depicted in red) point along the z' direction. The primed coordinates are obtained from a rotation of the coordinate system denoted by x , y , and z via a rotation around the x axis [44].

following Holstein-Primakoff and Fourier transformation:

$$\begin{aligned}
 \hat{S}_j^+ &= \sqrt{\frac{2S}{N}} \sum_k e^{-ik \cdot r} \hat{a}_k^\dagger, & \hat{S}_i^+ &= \sqrt{\frac{2S}{N}} \sum_k e^{ik \cdot r} \hat{b}_k, \\
 \hat{S}_j^- &= \sqrt{\frac{2S}{N}} \sum_k e^{ik \cdot r} \hat{a}_k, & \hat{S}_i^- &= \sqrt{\frac{2S}{N}} \sum_k e^{-ik \cdot r} \hat{b}_k^\dagger, \\
 \hat{S}_j^{z'} &= -S + \frac{1}{N} \sum_{k,k'} e^{-i(k-k') \cdot r} \hat{a}_k^\dagger \hat{a}_{k'}, \\
 \hat{S}_i^{z'} &= S - \frac{1}{N} \sum_{k,k'} e^{-i(k-k') \cdot r} \hat{b}_k^\dagger \hat{b}_{k'},
 \end{aligned} \quad (D2)$$

where index $i(j)$ denotes a lattice site belonging to sublattice $A(B)$ and with $\hat{S}_i^\pm = \hat{S}_i^x \pm i\hat{S}_i^y$ and $\hat{S}_j^\pm = \hat{S}_j^x \pm i\hat{S}_j^y$. The directions y' , y'' , z' , and z'' can be obtained via a rotation around the x axis [44] and are schematically depicted in the canted ground state of hematite in Fig. 7. The operators \hat{a}^\dagger (\hat{b}^\dagger) denote the creation operators of spin-up (down) sublattice magnons. Applying this transformation [Eq. (D2)] to the Hamiltonian $\hat{\mathcal{H}}_{\text{hem}}$ leads to the following expression in terms of sublattice magnons:

$$\begin{aligned}
 \hat{\mathcal{H}}_{\text{hem}} &= \sum_k [A \hat{a}_k^\dagger \hat{a}_k + B \hat{b}_k^\dagger \hat{b}_k + C_k (\hat{a}_k \hat{b}_{-k} + \hat{a}_k^\dagger \hat{b}_{-k}^\dagger) \\
 &\quad + D (\hat{a}_k \hat{a}_{-k} + \hat{b}_k \hat{b}_{-k} + \hat{a}_k^\dagger \hat{a}_{-k}^\dagger + \hat{b}_k^\dagger \hat{b}_{-k}^\dagger) \\
 &\quad + E_k (\hat{a}_k \hat{b}_k^\dagger + \hat{a}_k^\dagger \hat{b}_k)],
 \end{aligned} \quad (D3)$$

With

$$\begin{aligned}
 A &\approx JS_z + KS, & D &= \frac{KS}{2}, \\
 B &\approx JS_z + KS, & E_k &= \phi DS_z \gamma_k, \\
 C_k &= JS_z \gamma_k, & \phi &= \frac{-\gamma \mu_0 \hbar H_0 - DS_z}{2JS_z},
 \end{aligned} \quad (D4)$$

where z is the number of nearest neighbors.

Finally, assuming a nanomagnet and taking only into account the $\mathbf{k} = \mathbf{0}$ mode [67,84], it follows $\gamma_k = 1$ and we define $\hat{a} \equiv \hat{a}_0$, $\hat{b} \equiv \hat{b}_0$, $C \equiv C_0$, $E \equiv E_0$. Our Hamiltonian describing hematite $\hat{\mathcal{H}}_{\text{hem}}$ [Eq. (D3)] becomes

$$\begin{aligned}
 \hat{\mathcal{H}}_{\text{hem}} &= A \hat{a}^\dagger \hat{a} + B \hat{b}^\dagger \hat{b} + C (\hat{a} \hat{b} + \hat{a}^\dagger \hat{b}^\dagger) \\
 &\quad + D (\hat{a}^2 + \hat{b}^2 + \hat{a}^{\dagger 2} + \hat{b}^{\dagger 2}) + E (\hat{a} \hat{b}^\dagger + \hat{a}^\dagger \hat{b}).
 \end{aligned} \quad (D5)$$

It is now evident that $\hat{\mathcal{H}}_{\text{hem}}$ [Eq. (D5)] contains extra terms $\hat{a} \hat{b}^\dagger$, $\hat{a}^\dagger \hat{b}$ that are spin nonconserving in comparison with the NiO Hamiltonian \hat{H}_{NiO} [Eq. (A5)]. We now want to tackle the question how our previous theory analysis changes when incorporating more spin nonconserving terms $\propto (\hat{a} \hat{b}^\dagger + \hat{a}^\dagger \hat{b})$.

We start by applying the Bogoliubov transformation [Eq. (A6)] on $\hat{\mathcal{H}}_{\text{hem}}$ [Eq. (D5)], such that

$$\begin{aligned}
 \hat{\mathcal{H}}_{\text{hem}} &= \omega (\hat{\alpha}^\dagger \hat{\alpha} + \hat{\beta}^\dagger \hat{\beta}) - \tilde{D}_r (\hat{\alpha} \hat{\beta}^\dagger + \hat{\alpha}^\dagger \hat{\beta}) \\
 &\quad + \tilde{D}_s (\hat{\alpha}^2 + \hat{\alpha}^{\dagger 2} + \hat{\beta}^2 + \hat{\beta}^{\dagger 2}) + (\omega - A),
 \end{aligned} \quad (D6)$$

with the modified coupling strengths

$$\begin{aligned}
 \tilde{D}_r &= D \left(\sinh(2r) - \frac{E}{2D} \sinh(2r) \right), \\
 \tilde{D}_s &= D \left(\cosh(2r) - \frac{E}{D} \cosh(2r) \right).
 \end{aligned} \quad (D7)$$

Our analysis from Appendixes A 2, B, and C can therefore be conveniently applied to hematite by substituting $D_r \rightarrow \tilde{D}_r$ and $D_s \rightarrow \tilde{D}_s$.

APPENDIX E: ROTATION TRANSFORMATION FOR PSEUDOSPIN

In this Appendix, we demonstrate the relations $\hat{\psi}_s = \hat{R}_y(\theta) \hat{\alpha} \hat{R}_y^\dagger(\theta)$ and $\hat{\psi}_a = \hat{R}_y(\theta) \hat{\beta} \hat{R}_y^\dagger(\theta)$ from Eq. (A17) with the rotation matrix $\hat{R}_y(\theta) = \exp(-i\theta \hat{L}_y)$ and the pseudospin component $\hat{L}_y = \frac{i}{2} (\hat{\alpha} \hat{\beta}^\dagger - \hat{\alpha}^\dagger \hat{\beta})$. From the Baker-Campbell-Hausdorff formula [99] follows

$$e^{\hat{A}} \hat{\alpha} e^{-\hat{A}} = \hat{\alpha} + [\hat{A}, \hat{\alpha}] + \frac{1}{2} [\hat{A}, [\hat{A}, \hat{\alpha}]] + \dots \quad (E1)$$

$$= \hat{\alpha} + \sum_{n=1} \frac{1}{n!} [\hat{A}, \hat{\alpha}]_n, \quad (E2)$$

where $[\hat{A}, \hat{\alpha}]_n$ is the n -fold nested commutator $[\hat{A}, \hat{\alpha}]_n = [\hat{A}, [\hat{A}, \hat{\alpha}]_{n-1}]$ and $[\hat{A}, \hat{\alpha}]_1 = [\hat{A}, \hat{\alpha}]$. Our rotation operations $\hat{\psi}_s = \hat{R}_y(\theta) \hat{\alpha} \hat{R}_y^\dagger(\theta)$ and $\hat{\psi}_a = \hat{R}_y(\theta) \hat{\beta} \hat{R}_y^\dagger(\theta)$ from Eq. (A17) can be expressed with the expansion expansion in Eq. (E2). Let us define for convenience $\hat{A} = \frac{\theta}{2} (\hat{\alpha} \hat{\beta}^\dagger - \hat{\alpha}^\dagger \hat{\beta})$ and deter-

mine $[\hat{A}, \hat{\alpha}]_n$. We find

$$[\hat{A}, \hat{\alpha}]_n = \begin{cases} \left(\frac{\theta}{2}\right)^{2k+1} (-1)^k \hat{\beta} & \text{for } n = 2k + 1, \\ \left(\frac{\theta}{2}\right)^{2k} (-1)^k \hat{\alpha} & \text{for } n = 2k, \end{cases} \quad (\text{E3})$$

with $k \in \mathbb{N}$. This can be shown with mathematical induction. Let us start with $n = 1$,

$$[\hat{A}, \hat{\alpha}]_1 = \frac{\theta}{2} [(\hat{\alpha} \hat{\beta}^\dagger - \hat{\alpha}^\dagger \hat{\beta}), \hat{\alpha}] = \frac{\theta}{2} \hat{\beta}, \quad (\text{E4})$$

and $n = 2$,

$$[\hat{A}, \hat{\alpha}]_2 = \left(\frac{\theta}{2}\right)^2 [(\hat{\alpha} \hat{\beta}^\dagger - \hat{\alpha}^\dagger \hat{\beta}), \hat{\beta}] = -\left(\frac{\theta}{2}\right)^2 \hat{\alpha}, \quad (\text{E5})$$

which is both in accordance with the formula for the nested commutator in Eq. (E3). We now perform the induction step for $n + 1$, where we have to make a distinction between $n + 1$ even and $n + 1$ odd. We begin with $n + 1 = 2k + 1$. The nested commutator for $2k + 1$ then reads

$$[\hat{A}, \hat{\alpha}]_{2k+1} = [\hat{A}, [\hat{A}, \hat{\alpha}]_{2k}] = \left(\frac{\theta}{2}\right)^{2k} (-1)^k [\hat{A}, \hat{\alpha}] \quad (\text{E6})$$

$$= \left(\frac{\theta}{2}\right)^{2k+1} (-1)^k \hat{\beta}, \quad (\text{E7})$$

which reproduces the formula in Eq. (E3). Now we take an even $n + 1 = 2k + 2$. The corresponding nested commutator reads

$$[\hat{A}, \hat{\alpha}]_{2k+2} = [\hat{A}, [\hat{A}, \hat{\alpha}]_{2k+1}] = \left(\frac{\theta}{2}\right)^{2k+1} (-1)^k [\hat{A}, \hat{\beta}] \quad (\text{E8})$$

$$= \left(\frac{\theta}{2}\right)^{2k+2} (-1)^{k+1} \hat{\alpha}, \quad (\text{E9})$$

which is also in accordance with the formula in Eq. (E3). We can now separate odd and even n in the expansion of $e^{\hat{A}} \hat{\alpha} e^{-\hat{A}}$ [Eq. (E2)], which becomes

$$e^{\hat{A}} \hat{\alpha} e^{-\hat{A}} = \hat{\alpha} + \sum_{k=1} \frac{1}{(2k)!} [\hat{A}, \hat{\alpha}]_{2k} + \sum_{k=0} \frac{1}{(2k+1)!} [\hat{A}, \hat{\alpha}]_{2k+1} \quad (\text{E10})$$

$$= \sum_{k=0} \frac{1}{(2k)!} \left(\frac{\theta}{2}\right)^{2k} (-1)^k \hat{\alpha} + \sum_{k=0} \frac{1}{(2k+1)!} \left(\frac{\theta}{2}\right)^{2k+1} (-1)^k \hat{\beta} \quad (\text{E11})$$

$$= \cos\left(\frac{\theta}{2}\right) \hat{\alpha} + \sin\left(\frac{\theta}{2}\right) \hat{\beta}. \quad (\text{E12})$$

With this we show

$$\hat{R}_y(\theta) \hat{\alpha} \hat{R}_y^\dagger(\theta) = \cos\left(\frac{\theta}{2}\right) \hat{\alpha} + \sin\left(\frac{\theta}{2}\right) \hat{\beta}, \quad (\text{E13})$$

and therefore

$$\hat{\psi}_s = \hat{R}_y(\theta) \hat{\alpha} \hat{R}_y^\dagger(\theta). \quad (\text{E14})$$

Under the same considerations, we can show that $\hat{\psi}_a = \hat{R}_y(\theta) \hat{\beta} \hat{R}_y^\dagger(\theta)$. Now the nested commutators become

$$[\hat{A}, \hat{\beta}]_n = \begin{cases} \left(\frac{\theta}{2}\right)^{2k+1} (-1)^{k+1} \hat{\alpha} & \text{for } n = 2k + 1, \\ \left(\frac{\theta}{2}\right)^{2k} (-1)^k \hat{\beta} & \text{for } n = 2k, \end{cases}$$

such that

$$\hat{R}_y(\theta) \hat{\beta} \hat{R}_y^\dagger(\theta) = \cos\left(\frac{\theta}{2}\right) \hat{\beta} - \sin\left(\frac{\theta}{2}\right) \hat{\alpha}, \quad (\text{E15})$$

from which follows indeed $\hat{\psi}_a = \hat{R}_y(\theta) \hat{\beta} \hat{R}_y^\dagger(\theta)$.

- [1] W. Heisenberg, Über den anschaulichen Inhalt der quantentheoretischen Kinematik und Mechanik, *Z. Phys.* **43**, 172 (1927).
- [2] C. Gerry, P. Knight, and P. L. Knight, *Introductory Quantum Optics* (Cambridge University Press, Cambridge, UK, 2005).
- [3] D. Walls and G. J. Milburn (eds.), *Quantum Optics* (Springer, Berlin, Heidelberg, 2008).
- [4] R. Schnabel, Squeezed states of light and their applications in laser interferometers, *Phys. Rep.* **684**, 1 (2017).
- [5] B. P. Abbott *et al.*, LIGO: the laser interferometer gravitational-wave observatory, *Rep. Prog. Phys.* **72**, 076901 (2009).
- [6] H. Grote, K. Danzmann, K. L. Dooley, R. Schnabel, J. Slutsky, and H. Vahlbruch, First long-term application of squeezed states of light in a gravitational-wave observatory, *Phys. Rev. Lett.* **110**, 181101 (2013).
- [7] J. Aasi *et al.*, Enhanced sensitivity of the LIGO gravitational wave detector by using squeezed states of light, *Nat. Photon.* **7**, 613 (2013).
- [8] G. J. Milburn and S. L. Braunstein, Quantum teleportation with squeezed vacuum states, *Phys. Rev. A* **60**, 937 (1999).
- [9] C. H. Bennett, G. Brassard, C. Crépeau, R. Jozsa, A. Peres, and W. K. Wootters, Teleporting an unknown quantum state

via dual classical and Einstein-Podolsky-Rosen channels, *Phys. Rev. Lett.* **70**, 1895 (1993).

- [10] J. C. Hoke *et al.* (Google Quantum AI and Collaborators), Measurement-induced entanglement and teleportation on a noisy quantum processor, *Nature (London)* **622**, 481 (2023).
- [11] R. E. Slusher, L. W. Hollberg, B. Yurke, J. C. Mertz, and J. F. Valley, Observation of squeezed states generated by four-wave mixing in an optical cavity, *Phys. Rev. Lett.* **55**, 2409 (1985).
- [12] L.-A. Wu, H. J. Kimble, J. L. Hall, and H. Wu, Generation of squeezed states by parametric down conversion, *Phys. Rev. Lett.* **57**, 2520 (1986).
- [13] H. Vahlbruch, M. Mehmet, K. Danzmann, and R. Schnabel, Detection of 15 dB squeezed states of light and their application for the absolute calibration of photoelectric quantum efficiency, *Phys. Rev. Lett.* **117**, 110801 (2016).
- [14] S. Steinlechner, J. Bauchrowitz, T. Eberle, and R. Schnabel, Strong Einstein-Podolsky-Rosen steering with unconditional entangled states, *Phys. Rev. A* **87**, 022104 (2013).
- [15] M. Ast, S. Steinlechner, and R. Schnabel, Reduction of classical measurement noise via quantum-dense metrology, *Phys. Rev. Lett.* **117**, 180801 (2016).

- [16] J. Hald, J. L. Sørensen, C. Schori, and E. S. Polzik, Spin squeezed atoms: A macroscopic entangled ensemble created by light, *Phys. Rev. Lett.* **83**, 1319 (1999).
- [17] A. Kuzmich, K. Mølmer, and E. S. Polzik, Spin Squeezing in an ensemble of atoms illuminated with squeezed light, *Phys. Rev. Lett.* **79**, 4782 (1997).
- [18] K. Hammerer, A. S. Sørensen, and E. S. Polzik, Quantum interface between light and atomic ensembles, *Rev. Mod. Phys.* **82**, 1041 (2010).
- [19] J. G. Bohnet, K. C. Cox, M. A. Norcia, J. M. Weiner, Z. Chen, and J. K. Thompson, Reduced spin measurement back-action for a phase sensitivity ten times beyond the standard quantum limit, *Nat. Photon.* **8**, 731 (2014).
- [20] J. G. Bohnet, B. C. Sawyer, J. W. Britton, M. L. Wall, A. M. Rey, M. Foss-Feig, and J. J. Bollinger, Quantum spin dynamics and entanglement generation with hundreds of trapped ions, *Science* **352**, 1297 (2016).
- [21] O. Hosten, R. Krishnakumar, N. J. Engelsen, and M. A. Kasevich, Quantum phase magnification, *Science* **352**, 1552 (2016).
- [22] O. Hosten, N. J. Engelsen, R. Krishnakumar, and M. A. Kasevich, Measurement noise 100 times lower than the quantum-projection limit using entangled atoms, *Nature (London)* **529**, 505 (2016).
- [23] X.-Y. Luo, Y.-Q. Zou, L.-N. Wu, Q. Liu, M.-F. Han, M. K. Tey, and L. You, Deterministic entanglement generation from driving through quantum phase transitions, *Science* **355**, 620 (2017).
- [24] Y.-Q. Zou, L.-N. Wu, Q. Liu, X.-Y. Luo, S.-F. Guo, J.-H. Cao, M. K. Tey, and L. You, Beating the classical precision limit with spin-1 Dicke states of more than 10,000 atoms, *Proc. Natl. Acad. Sci. USA* **115**, 6381 (2018).
- [25] H. Bao, J. Duan, S. Jin, X. Lu, P. Li, W. Qu, M. Wang, I. Novikova, E. E. Mikhailov, K.-F. Zhao, K. Mølmer, H. Shen, and Y. Xiao, Spin squeezing of 10^{11} atoms by prediction and retrodiction measurements, *Nature (London)* **581**, 159 (2020).
- [26] W. J. Eckner, N. Darkwah Oppong, A. Cao, A. W. Young, W. R. Milner, J. M. Robinson, J. Ye, and A. M. Kaufman, Realizing spin squeezing with Rydberg interactions in an optical clock, *Nature (London)* **621**, 734 (2023).
- [27] A. Kamra and W. Belzig, Super-poissonian shot noise of squeezed-magnon mediated spin transport, *Phys. Rev. Lett.* **116**, 146601 (2016).
- [28] A. Kamra, E. Thingstad, G. Rastelli, R. A. Duine, A. Brataas, W. Belzig, and A. Sudbø, Antiferromagnetic magnons as highly squeezed Fock states underlying quantum correlations, *Phys. Rev. B* **100**, 174407 (2019).
- [29] A. Kamra, W. Belzig, and A. Brataas, Magnon-squeezing as a niche of quantum magnonics, *Appl. Phys. Lett.* **117**, 090501 (2020).
- [30] H. Y. Yuan, S. Zheng, Z. Ficek, Q. Y. He, and M.-H. Yung, Enhancement of magnon-magnon entanglement inside a cavity, *Phys. Rev. B* **101**, 014419 (2020).
- [31] J. Zou, S. K. Kim, and Y. Tserkovnyak, Tuning entanglement by squeezing magnons in anisotropic magnets, *Phys. Rev. B* **101**, 014416 (2020).
- [32] D. Wuhler, N. Rohling, and W. Belzig, Theory of quantum entanglement and structure of the two-mode squeezed antiferromagnetic magnon vacuum, *Phys. Rev. B* **105**, 054406 (2022).
- [33] V. Azimi Mousolou, Y. Liu, A. Bergman, A. Delin, O. Eriksson, M. Pereiro, D. Thonig, and E. Sjöqvist, Magnon-magnon entanglement and its quantification via a microwave cavity, *Phys. Rev. B* **104**, 224302 (2021).
- [34] D. Wuhler, N. Rohling, and W. Belzig, Dipole-dipole-interaction-induced entanglement between two-dimensional ferromagnets, *Appl. Phys. Lett.* **125**, 022404 (2024).
- [35] T.-X. Lu, X. Xiao, L. S. Chen, Q. Zhang, and H. Jing, Magnon-squeezing-enhanced slow light and second-order sideband in cavity magnomechanics, *Phys. Rev. A* **107**, 063714 (2023).
- [36] D. Lachance-Quirion, Y. Tabuchi, A. Gloppe, K. Usami, and Y. Nakamura, Hybrid quantum systems based on magnonics, *Appl. Phys. Express* **12**, 070101 (2019).
- [37] G. Q. Yan, S. Li, H. Lu, M. Huang, Y. Xiao, L. Wernert, J. A. Brock, E. E. Fullerton, H. Chen, H. Wang, and C. R. Du, Quantum sensing and imaging of spin-orbit-torque-driven spin dynamics in the non-collinear antiferromagnet Mn_3Sn , *Adv. Mater.* **34**, 2200327 (2022).
- [38] D. Awschalom, C. Du, R. He, J. Heremans, A. Hoffmann, J. Hou, H. Kurebayashi, P. Li, L. Liu, V. Novosad, J. Sklenar, S. Sullivan, D. Sun, H. Tang, V. Tyberkevych, C. Trevillian, A. Tsen, L. Weiss, W. Zhang, and C. Zollitsch, Quantum engineering with hybrid magnonic systems and materials (Invited paper), *IEEE Trans. Quantum Eng.* **2**, 1 (2021).
- [39] J. Shim, S.-J. Kim, S. K. Kim, and K.-J. Lee, Enhanced magnon-photon coupling at the angular momentum compensation point of ferrimagnets, *Phys. Rev. Lett.* **125**, 027205 (2020).
- [40] C. Psaroudaki and C. Panagopoulos, Skyrmion qubits: A new class of quantum logic elements based on nanoscale magnetization, *Phys. Rev. Lett.* **127**, 067201 (2021).
- [41] C. A. Potts, E. Varga, V. A. S. V. Bittencourt, S. V. Kusminskiy, and J. P. Davis, Dynamical backaction magnomechanics, *Phys. Rev. X* **11**, 031053 (2021).
- [42] M. S. Ebrahimi, A. Motazedifard, and M. B. Harouni, Single-quadrature quantum magnetometry in cavity electromagnonics, *Phys. Rev. A* **103**, 062605 (2021).
- [43] A. Kamra, T. Wimmer, H. Huebl, and M. Althammer, Antiferromagnetic magnon pseudospin: Dynamics and diffusive transport, *Phys. Rev. B* **102**, 174445 (2020).
- [44] T. Wimmer, A. Kamra, J. Gückelhorn, M. Opel, S. Geprägs, R. Gross, H. Huebl, and M. Althammer, Observation of antiferromagnetic magnon pseudospin dynamics and the Hanle effect, *Phys. Rev. Lett.* **125**, 247204 (2020).
- [45] E. Kleinherbers and Y. Tserkovnyak, Magnon kinetic theory of the antiferromagnetic Hanle effect, *Phys. Rev. B* **110**, L140408 (2024).
- [46] P. Tang and Gerrit E. W. Bauer, Thermal and coherent spin pumping by noncollinear antiferromagnets, *Phys. Rev. Lett.* **133**, 036701 (2024).
- [47] A. Ross, R. Lebrun, L. Baldrati, A. Kamra, O. Gomonay, S. Ding, F. Schreiber, D. Backes, F. Maccheronzi, D. A. Grave, A. Rothschild, J. Sinova, and M. Kläui, An insulating doped antiferromagnet with low magnetic symmetry as a room temperature spin conduit, *Appl. Phys. Lett.* **117**, 242405 (2020).
- [48] J. Gückelhorn, S. de-la-Peña, M. Scheufele, M. Grammer, M. Opel, S. Geprägs, J. C. Cuevas, R. Gross, H. Huebl, A. Kamra, and M. Althammer, Observation of the nonreciprocal magnon Hanle effect, *Phys. Rev. Lett.* **130**, 216703 (2023).
- [49] L. Sheng, A. Duvakina, H. Wang, K. Yamamoto, R. Yuan, J. Wang, P. Chen, W. He, K. Yu, Y. Zhang, J. Chen, J. Hu, W.

- Song, S. Liu, X. Han, D. Yu, J.-P. Ansermet, S. Maekawa, D. Grundler, and H. Yu, Control of spin currents by magnon interference in a canted antiferromagnet, *Nat. Phys.* **21**, 740 (2025).
- [50] X. Ye and T. Yu, Magnon correlation enables spin injection, dephasing, and transport in canted antiferromagnets, *Phys. Rev. B* **112**, 224417 (2025).
- [51] S. C. Burd, R. Srinivas, H. M. Knaack, W. Ge, A. C. Wilson, D. J. Wineland, D. Leibfried, J. J. Bollinger, D. T. C. Allcock, and D. H. Slichter, Quantum amplification of boson-mediated interactions, *Nat. Phys.* **17**, 898 (2021).
- [52] J. Klein and F. M. Ross, Materials beyond monolayers: The magnetic quasi-1D semiconductor CrSBr, *J. Mater. Res.* **39**, 3045 (2024).
- [53] A. L. Melendez, S. Das, F. A. Rodriguez, I.-H. Kao, W. Liu, A. J. Williams, B. Lv, J. Goldberger, S. Chatterjee, S. Singh, and P. C. Hammel, Quantum sensing of broadband spin dynamics and magnon transport in antiferromagnets, *Sci. Adv.* **11**, eadu9381 (2025).
- [54] F. Keffer and C. Kittel, Theory of antiferromagnetic resonance, *Phys. Rev.* **85**, 329 (1952).
- [55] C. Kittel, *Quantum Theory of Solids* (Wiley, New York, NY, 1987).
- [56] V. Azimi-Mousolou, A. Bergman, A. Delin, O. Eriksson, M. Pereiro, D. Thonig, and E. Sjöqvist, Quantum spin systems: Toroidal classification and geometric duality, *Phys. Rev. B* **110**, L140403 (2024).
- [57] S. M. Rezende, A. Azevedo, and R. L. Rodríguez-Suárez, Introduction to antiferromagnetic magnons, *J. Appl. Phys.* **126**, 151101 (2019).
- [58] A.-L. E. Römling, Pseudospin squeezing (2025), https://github.com/alroemling/Pseudospin_squeezing.
- [59] H. Y. Yuan, W. P. Sterk, A. Kamra, and R. A. Duine, Master equation approach to magnon relaxation and dephasing, *Phys. Rev. B* **106**, 224422 (2022).
- [60] B. J. Dalton, J. Goold, B. M. Garraway, and M. D. Reid, Quantum entanglement for systems of identical bosons: II. Spin squeezing and other entanglement tests, *Phys. Scr.* **92**, 023005 (2017).
- [61] W. Zhang and K. M. Krishnan, Epitaxial exchange-bias systems: From fundamentals to future spin-orbitronics, *Mater. Sci. Eng.: Reports* **105**, 1 (2016).
- [62] A. Kamra and W. Belzig, Spin pumping and shot noise in ferrimagnets: Bridging ferro- and antiferromagnets, *Phys. Rev. Lett.* **119**, 197201 (2017).
- [63] A. Kamra, A. Rezaei, and W. Belzig, Spin splitting induced in a superconductor by an antiferromagnetic insulator, *Phys. Rev. Lett.* **121**, 247702 (2018).
- [64] S. A. Bender, R. A. Duine, and Y. Tserkovnyak, Electronic pumping of quasiequilibrium Bose-Einstein-condensed magnons, *Phys. Rev. Lett.* **108**, 246601 (2012).
- [65] J. Zheng, S. Bender, J. Armitis, R. E. Troncoso, and R. A. Duine, Green's function formalism for spin transport in metal-insulator-metal heterostructures, *Phys. Rev. B* **96**, 174422 (2017).
- [66] Anna Luisa E. Römling, A. Vivas-Viaña, C. S. Muñoz, and A. Kamra, Resolving nonclassical magnon composition of a magnetic ground state via a qubit, *Phys. Rev. Lett.* **131**, 143602 (2023).
- [67] Anna Luisa E. Römling and A. Kamra, Quantum sensing of antiferromagnetic magnon two-mode squeezed vacuum, *Phys. Rev. B* **109**, 174410 (2024).
- [68] The stability of the groundstate dictates $1 > 2|D_s/\omega| + \sqrt{(\chi/\omega)^2 + (D_r/\omega)^2}$.
- [69] Factor c_2 is given by $c_2 = -\frac{Ds/Dr}{8} \left(\frac{2(m+\frac{1}{2})a_+ \sinh(2r_+ - 2r_-)}{(m+\frac{1}{2}) \cosh(2r_+ - 2r_-) - \frac{1}{2}} - \frac{2(m+\frac{1}{2})a_- \sinh(2r_+ + 2r_-)}{(m+\frac{1}{2}) \cosh(2r_+ + 2r_-) - \frac{1}{2}} \right)$, with $a_{\pm} = \frac{1}{(\omega - D_r)^2 - 4D_s^2} \pm \frac{1}{(\omega + D_r)^2 - 4D_s^2}$ (see Appendix C 2).
- [70] T. S. Parvini, V. A. S. V. Bittencourt, and S. V. Kusminskiy, Antiferromagnetic cavity optomagnonics, *Phys. Rev. Res.* **2**, 022027(R) (2020).
- [71] W. Janus, T. Slezak, M. Ślęzak, M. Szyptma, P. Drózd, H. Nayyef, A. Mandziak, D. Wilgocka-Ślęzak, M. Zajac, M. Jugovac, T. Menteş, A. Locatelli, and A. Kozioł-Rachwał, Tunable magnetic anisotropy of antiferromagnetic NiO in (Fe)/NiO/MgO/Cr/MgO(001) epitaxial multilayers, *Sci. Rep.* **13**, 4824 (2023).
- [72] T. Jungwirth, X. Marti, P. Wadley, and J. Wunderlich, Antiferromagnetic spintronics, *Nat. Nanotechnol.* **11**, 231 (2016).
- [73] M. M. Nieto, Displaced and squeezed number states, *Phys. Lett. A* **229**, 135 (1997).
- [74] P. Král, Displaced and squeezed fock states, *J. Mod. Opt.* **37**, 889 (1990).
- [75] S. B. Korolev, E. N. Bashmakova, and T. Y. Golubeva, Error correction using squeezed Fock states, *Quantum Info. Proc.* **23**, 354 (2024).
- [76] T. Jungwirth, J. Wunderlich, V. Novák, K. Olejník, B. L. Gallagher, R. P. Campion, K. W. Edmonds, A. W. Rushforth, A. J. Ferguson, and P. Němec, Spin-dependent phenomena and device concepts explored in (Ga,Mn)As, *Rev. Mod. Phys.* **86**, 855 (2014).
- [77] S. M. Wu, S. A. Cybart, D. Yi, J. M. Parker, R. Ramesh, and R. C. Dynes, Full electric control of exchange bias, *Phys. Rev. Lett.* **110**, 067202 (2013).
- [78] T. Jungwirth, V. Novák, X. Martí, M. Cukr, F. Máca, A. B. Shick, J. Mašek, P. Horodyská, P. Němec, V. Holý, J. Zemek, P. Kužel, I. Němec, B. L. Gallagher, R. P. Campion, C. T. Foxon, and J. Wunderlich, Demonstration of molecular beam epitaxy and a semiconducting band structure for I-Mn-V compounds, *Phys. Rev. B* **83**, 035321 (2011).
- [79] B. Pradenas and O. Tchernyshyov, Spin-frame field theory of a three-sublattice antiferromagnet, *Phys. Rev. Lett.* **132**, 096703 (2024).
- [80] B. Pradenas, G. Adamyan, and O. Tchernyshyov, Spontaneous symmetry breaking in the Heisenberg antiferromagnet on a triangular lattice, *Phys. Rev. B* **112**, 104402 (2025).
- [81] M. T. Hutchings and E. J. Samuelsen, Measurement of spin-wave dispersion in NiO by inelastic neutron scattering and its relation to magnetic properties, *Phys. Rev. B* **6**, 3447 (1972).
- [82] S. M. Rezende, R. L. Rodríguez-Suárez, and A. Azevedo, Diffusive magnonic spin transport in antiferromagnetic insulators, *Phys. Rev. B* **93**, 054412 (2016).
- [83] T. Holstein and H. Primakoff, Field dependence of the intrinsic domain magnetization of a ferromagnet, *Phys. Rev.* **58**, 1098 (1940).
- [84] I. C. Skogvoll, J. Lidal, J. Danon, and A. Kamra, Tunable anisotropic quantum Rabi model via a magnon-spin-qubit ensemble, *Phys. Rev. Appl.* **16**, 064008 (2021).

- [85] H.-P. Breuer and F. Petruccione, *The Theory of Open Quantum Systems* (Oxford University Press, Oxford, UK, 2007).
- [86] S. A. Bender and Y. Tserkovnyak, Interfacial spin and heat transfer between metals and magnetic insulators, *Phys. Rev. B* **91**, 140402(R) (2015).
- [87] A. Kamra and W. Belzig, Magnon-mediated spin current noise in ferromagnet | nonmagnetic conductor hybrids, *Phys. Rev. B* **94**, 014419 (2016).
- [88] S. Takahashi, E. Saitoh, and S. Maekawa, Spin current through a normal-metal/insulating-ferromagnet junction, *J. Phys.: Conf. Ser.* **200**, 062030 (2010).
- [89] S. S.-L. Zhang and S. Zhang, Spin convertance at magnetic interfaces, *Phys. Rev. B* **86**, 214424 (2012).
- [90] D. I. Schuster, A. A. Houck, J. A. Schreier, A. Wallraff, J. M. Gambetta, A. Blais, L. Frunzio, J. Majer, B. Johnson, M. H. Devoret, S. M. Girvin, and R. J. Schoelkopf, Resolving photon number states in a superconducting circuit, *Nature (London)* **445**, 515 (2007).
- [91] D. Lachance-Quirion, Y. Tabuchi, S. Ishino, A. Noguchi, T. Ishikawa, R. Yamazaki, and Y. Nakamura, Resolving quanta of collective spin excitations in a millimeter-sized ferromagnet, *Sci. Adv.* **3**, e1603150 (2017).
- [92] S. Kono, Y. Masuyama, T. Ishikawa, Y. Tabuchi, R. Yamazaki, K. Usami, K. Koshino, and Y. Nakamura, Nonclassical photon number distribution in a superconducting cavity under a squeezed drive, *Phys. Rev. Lett.* **119**, 023602 (2017).
- [93] F. J. Morin, Magnetic susceptibility of α -Fe₂O₃ and α -Fe₂O₃ with added titanium, *Phys. Rev.* **78**, 819 (1950).
- [94] T. Dannegger, A. Deák, L. Rózsa, E. Galindez-Ruales, S. Das, E. Baek, M. Kläui, L. Szunyogh, and U. Nowak, Magnetic properties of hematite revealed by an *ab initio* parameterized spin model, *Phys. Rev. B* **107**, 184426 (2023).
- [95] V. V. Mazurenko and V. I. Anisimov, Weak ferromagnetism in antiferromagnets: α -Fe₂O₃ and La₂CuO₄, *Phys. Rev. B* **71**, 184434 (2005).
- [96] C. Kittel, *Introduction to Solid State Physics* (John Wiley & Sons, New York, NY, 2015).
- [97] A. Ross, R. Lebrun, O. Gomonay, J. Sinova, A. Kay, D. A. Grave, A. Rothschild, and M. Kläui, Magnon transport in the presence of antisymmetric exchange in a weak antiferromagnet, *J. Magn. Magn. Mater.* **543**, 168631 (2022).
- [98] I. Boverter, H. T. Simensen, B. Brekke, M. Weides, A. Anane, M. Kläui, A. Brataas, and R. Lebrun, Antiferromagnetic cavity magnon polaritons in collinear and canted phases of hematite, *Phys. Rev. Appl.* **19**, 014071 (2023).
- [99] H. F. Baker, On the exponential theorem for a simply transitive continuous group, and the calculation of the finite equations from the constants of structure, *Proc. London Math. Soc.* **s1-34**, 91 (1901).